Indian J Phys (July 2017) 91(7):779–802
DOI 10.1007/s12648-017-0970-x

ORIGINAL PAPER

Spectroscopic and Raman excitation profile studies of 3-benzoylpyridine

P Sett[1]*, S Datta[2], J Chowdhury[3], M Ghosh[4] and P K Mallick[2]

[1]Department of Physics, Gobardanga Hindu College, North 24, Pargana, West Bengal 743273, India

[2]Department of Physics, Burdwan University, Burdwan, West Bengal 713104, India

[3]Department of Physics, Jadavpur University, Jadavpur, Kolkata, West Bengal 700032, India

[4]Department of Spectroscopy, Indian Association for the Cultivation of Science, Kolkata, West Bengal 700032, India

Received: 07 March 2016 / Accepted: 23 December 2016 / Published online: 14 March 2017

Abstract: In the present work IR, UV absorption and Raman spectra including Raman excitation profiles and structure of 3-benzoyl pyridine have been investigated. Detailed studies on the vibrational and electronic properties of the molecule have been carried out. All these studies are aided with valuable quantum chemical calculations. The structural changes encountered on excitation to the low lying excited states have been investigated. Theoretical profiles determined by the sum-over-states method based on pertinent Franck–Condon and Herzberg–Teller terms have satisfactorily simulated the experimentally measured relative Raman intensities and these are also in compliance with the structural changes and potential energy distributions.

Keywords: Vibrational spectra; Raman excitation profile; Sum-overstates method; Excited electronic state; Molecular configuration

PACS Nos: 33.20.Fb; 33.20.Tp; 36.20.Kd; 36.20.Ng

1. Introduction

In Raman scattering two factors play dominant roles in determining the intensity, namely Franck–Condon (FC) and vibronic or Herzberg–Teller coupling (VC or HT) mechanisms. The former mechanism depends on the displacement of the potential minimum of an excited allowed electronic state with respect to the ground state and the latter one on the vibronic coupling between two electronic states through the concerned normal mode. When the excitation lies in the resonance region, the FC factors are dominant and the analyses yield structural and conformational information of the resonant excited state. On the other hand for excitation in the off resonance region, both the mechanisms play important roles. So studies of the Raman excitation profiles of different normal modes for excitation in this region are expected to yield valuable information of molecules in their excited electronic states.

Simultaneous presence of some low-lying singlet and triplet ($n\pi^*$ and $\pi\pi^*$) states controls the photophysical behavior of aromatic and heterocyclic molecules [1–5]. To investigate this effect also on the vibrational properties, the present work deals with detailed study on the electronic and vibrational properties of 3-benzoyl pyridine, to complete the gamut of our investigation on the three isomers (2-, 3- and 4-) of benzoylpyridine (BOP) and 2,2'-dipyridyl ketone (2,2′-DPK) [6–9]. All these studies are aided with valuable quantum chemical calculations. In this communication, experimentally measured relative Raman intensities have also been simulated satisfactorily using the theoretical profiles determined by the sum-over-states method based on pertinent FC and VC terms.

2. Experimental and computational procedure

2.1. Chemicals

3-BOP was purchased from Aldrich Chemical Company, USA, with purity grade 98% and is used after checking its

*Corresponding author, E-mail: pinakysett@gmail.com

purity by HPLC. Spectroscopic-grade solvents carbon tetrachloride ($CHCl_3$), chloroform (CCl_4), methyl cyclohexane (MCH), cyclohexane (CHX) and ethanol (EtOH) were supplied by S.L.R., India, and are used as such. To record Raman and electronic absorption spectra, the concentrations of the solutions are maintained within the range 1–10^{-2} and 10^{-3}–10^{-6} M, respectively.

2.2. Instrumentation

The electronic absorption spectra are recorded with a Shimadzu UV–VIS spectrophotometer (Model UV 1800). The infrared spectra of thin films are recorded on a previously calibrated Perkin-Elmer Model 783 infrared spectrophotometer. The resolution of the infrared bands is about 2 cm^{-1} for sharp bands and slightly less for the broader ones. Raman spectra of the samples in pure form and in chloroform and carbon tetrachloride solutions are recorded with a Spex Raman Spectrophotometer (RAMALOG), interfaced with a computer in the photon counting mode and fitted with an Ar^+ ion laser using 514.5, 501.7, 496.5, 488.0, 476.5 and 457.9 nm as exciting wavelengths. The holographic grating in this instrument with 1800 grooves/mm is mounted in a modified Czerny–Turner configuration. The slit widths of the monochromators are adjusted to obtain reasonably good Raman spectra. The detection system used is a photomultiplier tube (R928-7) from Hamamatsu Photonics K. K. (Japan), attached to the spectrometer and is held in a cryostat (Spex # 1730) with suitable resistor network. The tube has high quantum efficiency and uniform sensitivity over the range 400–800 nm, which is the usual region for detection of the scattered radiation. Polarized Raman spectra are recorded with an arrangement provided with the instrument. The accuracy of the measurements is ± 1 cm^{-1} for the strong and sharp bands and slightly less for the other bands.

The reference lines 267, 373 and 674 cm^{-1} for $CHCl_3$ and 220, 324 and 466 cm^{-1} for CCl_4 have been used as internal standards. Same procedure, as described in the earlier publications [8, 9] has been followed here to determine the variation of relative intensity of different Raman bands with exciting frequency for each reference line. For the measurement of REPs, Raman intensity of each band is normalized relative to that for the exciting wavelength at 514.5 nm and also the excitation frequency dependence of the intensity of the solvent band, used as internal standard, has been taken into consideration. Average of the results found on the basis of measurements with respect to the three internal standards in each solution has been compared with the theoretical curves.

The relative intensity of each Raman band of frequency (ν_a) corresponding to an exciting frequency (ν_{exc}) is given by,

$$\begin{aligned} I_{rel}(\nu_a, \nu_{exc}) &= I(\nu_a, \nu_{exc})/I(\nu_{IS}, \nu_{514.5}) \\ &= [I(\nu_a, \nu_{exc})/I(\nu_{IS}, \nu_{exc})] \\ &\times [I(\nu_{IS}, \nu_{exc})/I(\nu_{IS}, \nu_{514.5})] \\ &= [I(\nu_a, \nu_{exc})/I(\nu_{IS}, \nu_{exc})] \\ &\times [(\nu_{exc} - \nu_{IS})/(\nu_{514.5} - \nu_{IS})]^3 \end{aligned} \quad (1)$$

where all the intensities (I's) are measured in terms of the number of photons per second per scan. Thus ν^3 dependence has been taken into consideration. $\nu_{514.5}$ is the frequency of the exciting radiation of wavelength 514.5 nm and ν_{IS} is the frequency of the reference Raman band used as internal standard. For theoretical calculation of Raman intensities, see the section on Raman excitation profile below.

2.3. Theoretical calculations

Theoretical calculations are performed using the Gaussian 03 suit of program [10]. Structural optimization and calculation of the vibrational wavenumbers of the molecule for the optimized geometry have been carried out by density functional level of theory (DFT) using the Pople split valance polarization basis set 6-311G(d,p) with B3LYP [(i.e. Becke three hybrid exchange and Lee–Yang–Parr correlation functional (LYP)]. The B3PW91 functional with non-local correlation provided by Predew-Wang (PW) has also been utilized in the DFT calculation in conjunction with the same basis set and the two results are compared. In the process of geometry optimization for the fully relaxed method, convergence of all calculations and the absence of imaginary values in the wavenumbers of the normal modes confirm the attainment of global minima on the potential energy surface (PES). In order to fit the theoretical wavenumbers with the experimental ones, an overall scaling factor is introduced by using a least square optimization technique. For theoretical estimation of the FC transition energies of the molecule and their respective oscillator strengths, the method based on the time dependent density functional theory (TD-DFT) has been employed using integral equation formalism of the polarization continuum model (IEF-PCM) at the optimized B3LYP/6-311G(d,p) ground-state geometry. Calculations are carried out for vacuum/gas phase and also for different solvents like cyclohexane (CHX) and EtOH. An attempt is also made to calculate the FC transition energies at the configuration interaction single (CIS)/6-311G(d,p) level of theory, but the result has not been found to be satisfactory. The assignments of different normal modes are made on the basis of the corresponding potential energy distributions (PEDs) and the animated views of the respective normal modes. The PEDs are computed from the quantum chemically

estimated outcome using the GAR2PED program [11], a Gaussian 94 output post-processing utility program. As the results of the DFT approach with B3LYP correlated functional and 6311G(d,p) basis set reproduce the vibrational wavenumbers, well compatible with the observed ones, the Gaussian output file of this has been chosen as the input data of the GAR2PED computation. The Gauss View 3.0 program has been utilized to get visual animation and also for inspection of the normal mode description.

3. Results and discussion

3.1. Molecular geometry of 3-BOP

The interaction between the lone pair electrons of the ring nitrogen and substituent oxygen atoms is important in determining the structural features which in turn might be helpful in getting insight into the photophysical behaviour of the molecule. The ground-state structure of the titled molecule (3-BOP) is optimized by DFT calculation. By allowing relaxation of all the parameters, realistic optimized geometries, which correspond to true energy minima, have been achieved and realized by noting the absence of imaginary values of the calculated vibrational wavenumbers. To calculate the true optimized geometry we have started from different initial structures: phenyl ring is perpendicular to the pyridine ring (separately for (i) CIS and (ii) Trans configurations) with carbonyl group lying in the pyridyl ring plane; (iii) pyridyl ring is perpendicular to phenyl ring with carbonyl group lying in the phenyl ring plane; two rings are asymmetrically oriented about the C=O axis for both (iv) CIS and (v) TRANS configuration and (vi) two rings are oriented symmetrically about CO ring plane. These initial structure levels are respectively represented by A, B, C, D, E and F in the first column of Table 1. But in all cases, it has been observed that the two rings are oriented asymmetrically with respect to the carbonyl group in the final optimized structures of the molecule. The optimized geometries give rise to two configurations, namely TRANS and CIS, the minimum energies of which are found to be -592.8131 and -592.8123 Hartree (Table 1) i.e. TRANS conformer is more stable than the CIS form by about 2.10 kJ/mol (ΔE). Selected optimized parameters of the molecule are presented in Table 2 for the minimum energies of both TRANS and CIS configurations. Due to unavailability of the experimental data, the structural parameters, calculated theoretically, are compared with those obtained from the studies of similar type of molecules. Bond lengths, angles and torsional angles of the phenyl and pyridyl rings are comparable with those found in the structures of benzophenone (BP) [6], di(2-pyridyl)ketone (2,2′-DPK) [7], phenyl-2-pyridylketone (2-BOP) [8] and phenyl-4-pyridylketone (4-BOP) [9]. The B3LYP/6-311G(d,p) calculated optimized geometries of the two conformers (TRANS and CIS) of 3-BOP molecule, together with atom numbering, are shown in Figs. 1(a), 1(c) and 1(b), 1(d) respectively because both the structural parameter and wavenumber matching with the observed values are better for this level of theory than the B3PW91 functional. The phenyl ring remains more or less hexagonal for both CIS and TRANS isomers. The $C_R(C{=}O)C_R$ group is also found to be planar. However the two rings are not oriented symmetrically in the CIS structure, but in the TRANS structure the orientation of the two rings are more or less symmetrical with respect to the plane containing the carbonyl group. The angle between the two ring planes is about 53° for the CIS structure and 51° for the TRANS structure. These angles may be compared with those in BP [6], 2,2′-DPK [7] or 4-BOP [9] for which the dihedral angle between the ring planes are 60°, 45° and 50° respectively. The previous investigation shows that the angles of 2-BOP [8] are about 60° and 30° for the CIS and TRANS structure, respectively. In any case the two rings are not in the same plane with that containing the carbonyl group. So for both the conformers, the molecule does not have any plane of symmetry and so group symmetry is taken to be (C_1). Another point is interesting to note that the two bonds C_6-C_7 and C_7-C_8 are more or less equal in length as in the case of benzophenone [6] and 2,2′-DPK [7], although for the latter the bond lengths are to some extent greater. But this is not so for the other two isomers, 2-BOP [8] and 4-BOP

Table 1 Optimized potential energy of 3-BOP in different configurations

Initial structure level	Final structural configuration	Optimized potential energies (a.u.)	Angle between two ring planes
A	CIS	−592.81226121	52°
B	TRANS	−592.81314727	51°
C	TRANS	−592.81314786	51°
D	CIS	−592.81226184	54°
E	TRANS	−592.81314729	51°
F	CIS	−592.81314729	53°

Table 2 Equilibrium geometries of 3-BOP in internal coordinate system

	Ring-1			Ring-2		
		CIS	TRANS		CIS	TRANS
Atomic distances (in A^0)						
$R_{CC/CN}$	$R(C_1–N_2/C_1–C_2)$	1.332	1.386	$R(C_8–C_9)$	1.401	1.401
	$R(C_1–C_6)$	1.403	1.399	$R(C_9–C_{10})$	1.393	1.393
	$R(C_5–C_6)$	1.397	1.400	$R(C_{10}–C_{11})$	1.393	1.393
	$R(C_4–C_5/N_4–C_5)$	1.391	1.336	$R(C_{11}–C_{12})$	1.396	1.396
	$R(C_3–C_4/C_3–N_4)$	1.392	1.335	$R(C_{12}–C_{13})$	1.389	1.388
	$R(N_2–C_3/C_2–C_3)$	1.338	1.395	$R(C_{13}–C_8)$	1.402	1.402
R_{CH}	$R(C_1–H_{22})$	1.085	1.083	$R(C_9–H_{18})$	1.083	1.079
	$R(C_3–H_{21}/C_3–H_{20})$	1.086	1.087	$R(C_{10}–H_{17})$	1.084	1.084
	$R(C_4–H_{20}/C_2–H_{21})$	1.083	1.083	$R(C_{11}–H_{16})$	1.084	1.085
	$R(C_5–H_{19})$	1.083	1.085	$R(C_{12}–H_{15})$	1.084	1.084
				$R(C_{13}–H_{14})$	1.083	1.083
R_{CX}	$R(C_6–C_7)$	1.500	1.501	$R(C_8–C_7)$	1.500	1.498
Angles						
$A_{CCC/CCN/CNC}$	$A(C_1N_2C_3/C_1C_2C_3)$	117.32°	118.44°	$A(C_8C_9C_{10})$	120.29°	120.28°
	$A(N_2C_3C_4/C_2C_3N_4)$	123.57°	123.59°	$A(C_9C_{10}C_{11})$	120.07°	120.08°
	$A(C_3C_4C_5/C_3N_4C_5)$	118.57°	117.40°	$A(C_{10}C_{11}C_{12})$	119.98°	119.99°
	$A(C_4C_5C_6/N_4C_5C_6)$	118.87°	123.86°	$A(C_{11}C_{12}C_{13})$	120.03°	120.02°
	$A(C_5C_6C_1)$	117.63°	117.61°	$A(C_{12}C_{13}C_8)$	120.44°	120.44°
	$A(C_6C_1C_2)$	124.02°	119.06°	$A(C_{13}C_8C_9)$	119.17°	119.17°
$A_{CCH/NCH}$	$A(N_2C_1H_{22}/C_1C_2H_{22})$	117.00°	121.93°	$A(C_8C_9H_{18})$	120.08°	120.14°
	$A(C_6C_1H_{22})$	118.98°	119.00°	$A(C_{10}C_9H_{18})$	119.60°	119.56°
	$A(N_2C_3H_{21}/C_2C_3H_{20})$	116.00°	120.41°	$A(C_9C_{10}H_{17})$	119.82°	119.79°
	$A(C_4C_3H_{21}/N_4C_3H_{20})$	120.43°	116.00°	$A(C_{11}C_{10}H_{17})$	120.11°	120.13°
	$A(C_3C_4H_{20}/C_1C_2H_{21})$	120.34°	121.26°	$A(C_{10}C_{11}H_{16})$	119.99°	119.98°
	$A(C_5C_4H_{20}/C_3C_2H_{21})$	121.09°	120.30°	$A(C_{12}C_{11}H_{16})$	120.03°	120.03°
	$A(C_4C_5H_{19}/N_4C_5H_{19})$	120.53°	115.78°	$A(C_{11}C_{12}H_{15})$	120.04°	120.04°
	$A(C_6C_5H_{19})$	120.59°	120.35°	$A(C_{13}C_{12}H_{15})$	119.93°	119.93°
				$A(C_{12}C_{13}H_{14})$	121.13°	121.11°
				$A(C_8C_{13}H_{14})$	118.43°	118.45°
A_{CCX}	$A(C_1C_6C_7)$	118.32°	118.52°	$A(C_9C_8C_7)$	122.90°	122.93°
	$A(C_5C_6C_7)$	123.92°	123.67°	$A(C_{13}C_8C_7)$	117.82°	117.79°
Selected dihedral angles						
$D_{CCCC/CCCO/CNCC/NCCO}$	$D(N_2/C_2C_1C_6\ C_7)$	−177.50°	−177.17°	$D(C_{10}C_9C_8C_7)$	176.69°	176.59°
	$D(C_4/N_4C_5C_6C_7)$	176.18°	177.17°	$D(C_{12}C_{13}C_8C_7)$	−177.88°	−177.81°
	$D(C_1C_6C_7C_8)$	−150.76°	−153.84°	$D(C_9C_8C_7C_6)$	29.18°	29.74°
	$D(C_5C_6C_7C_8)$	33.45°	31.29°	$D(C_{13}C_8C_7C_6)$	−154.61°	−154.15°
	$D(C_1C_6C_7O_{23})$	29.33°	26.34°	$D(C_9C_8C_7O_{23})$	−150.92°	−150.44°
	$D(C_5C_6C_7O_{23})$	−146.45°	−148.53°	$D(C_{13}C_8C_7O_{23})$	25.29°	25.67°
Substitute						
Atomic distances (in A^0)						
R_{CO}	$R(C_7–O_{23})$	1.218	1.219			
Angles						
A_{CCC}	$A(C_6C_7C_8)$	120.13°	120.44°			
A_{CCO}	$A(C_6C_7O_{23})$	119.54°	119.27°			
	$A(C_8C_7O_{23})$	120.34°	120.29°			
Dihedral angle						
D_{CCOC}	$D(C_6C_7O_{23}C_8)$	179.90°	179.82°			

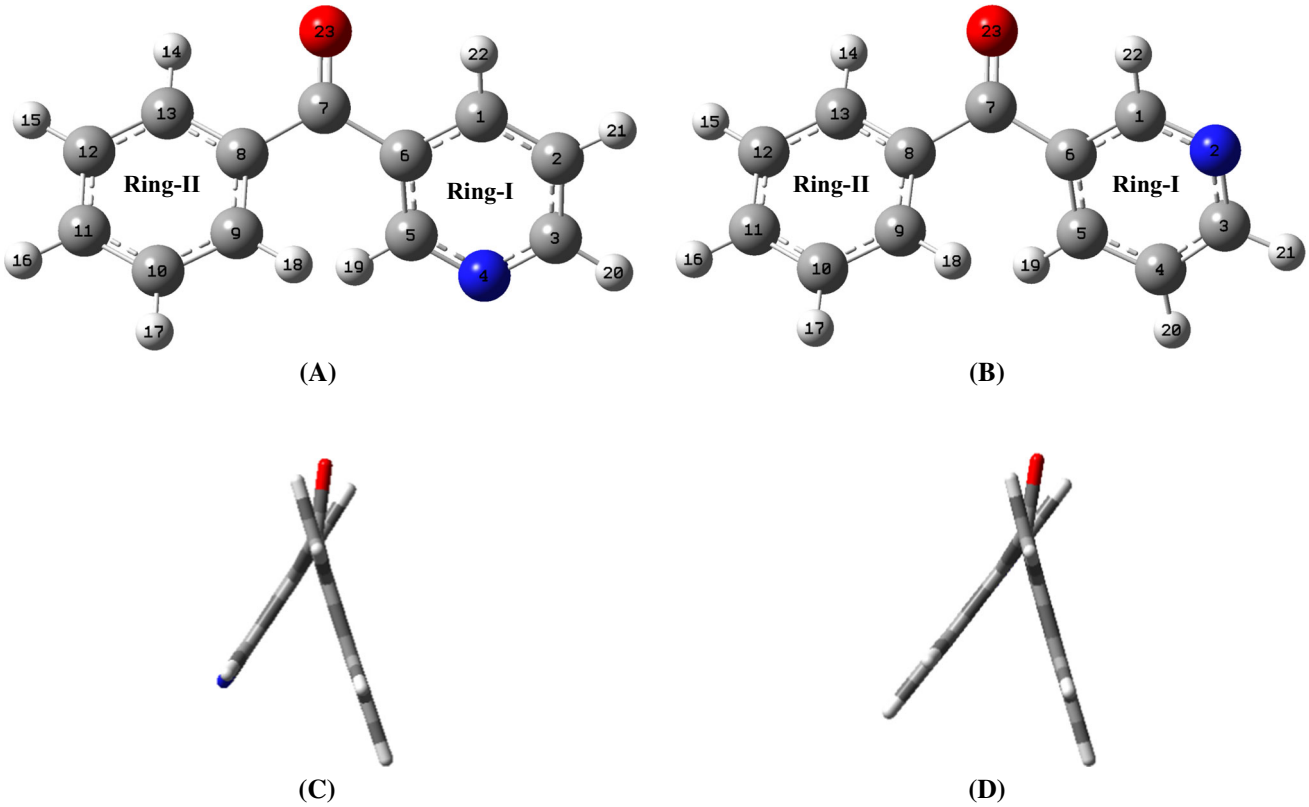

Fig. 1 Optimized ground state geometry [DFT//B3LYP/6-311G(d, p)] of 3-BOP molecule with atom numbering of (**a**) TRANS, (**b**) CIS configuration. Angular orientation between the ring planes is shown in (**c**) for TRANS and (**d**) for CIS configuration

[9] for which the difference in these bond lengths are about 0.02 and 0.01 Å respectively.

3.2. Vibrational Assignment

Under the point group C_1 all the vibrations (63 normal modes) of the molecule are expected to be both Raman and infrared active. The analysis of the vibrational spectra of such a big molecule is not trivial. However it becomes not only much simpler but more realistic, if we consider the molecule as a substituted pyridine (3X-C_5H_4N, where the substituent is (C=O)Φ, Φ being the phenyl group). In that case the 27 normal modes of the pyridine (under the point group C_S) are divided into the symmetry species $19A' + 8A''$. The molecule may also be considered as a substituted benzene molecule, C_6H_5X (X being the substituent (C=O)Π and Π being the pyridine ring). In that case the molecule belongs to the point group C_{2V} and the 30 normal modes are divided into the symmetry species as $11A_1 + 3A_2 + 6B_1 + 10B_2$. In both cases these normal modes are combined with those of the substituent group and make the total number 63 as mentioned above. This approach has been utilized previously by many workers [12–16]. Any way in the present case we have indicated the pyridyl ring as ring I and the phenyl ring as ring II.

The wavenumbers of the bands observed in the Raman spectra (Fig. 2) of the molecule in different environments are listed in Table 3 along with the infrared counterparts. Theoretically calculated spectral wavenumbers of both the isomers, CIS and TRANS (along with their respective potential energy distributions, PEDs), are shown in the Table 3. Since the calculated values overestimate both the harmonic force constants and hence the wavenumbers due to combination of electron correlation effects and basis set deficiencies, it is a usual method to scale down the calculated values for comparison with the observed wave numbers. Here we have used a uniform scaling factor 0.9677 for B3LYP and 0.9645 for B3PW91 functionals. Moreover since the calculated values correspond to those of the vapour state, so in spite of the scaling down, they will differ to some extent from the experimental ones observed in the solid state or in solutions.

To get a complete picture of the normal modes, a comparative study is made with benzophenone (BP) [6], 2- and 4-benzoyl pyridine (2- and 4-BOP) [8, 9], 2,2′-dipyridyl ketone (2,2′-DPK) [7]. Available literatures concerning vibrational assignments of similar types of molecules are also consulted in order to make a good and realistic assignment [12–14]. Previously, Mautner and Goher [15] and Chowdhury and Ghosh [16] observed vibrational

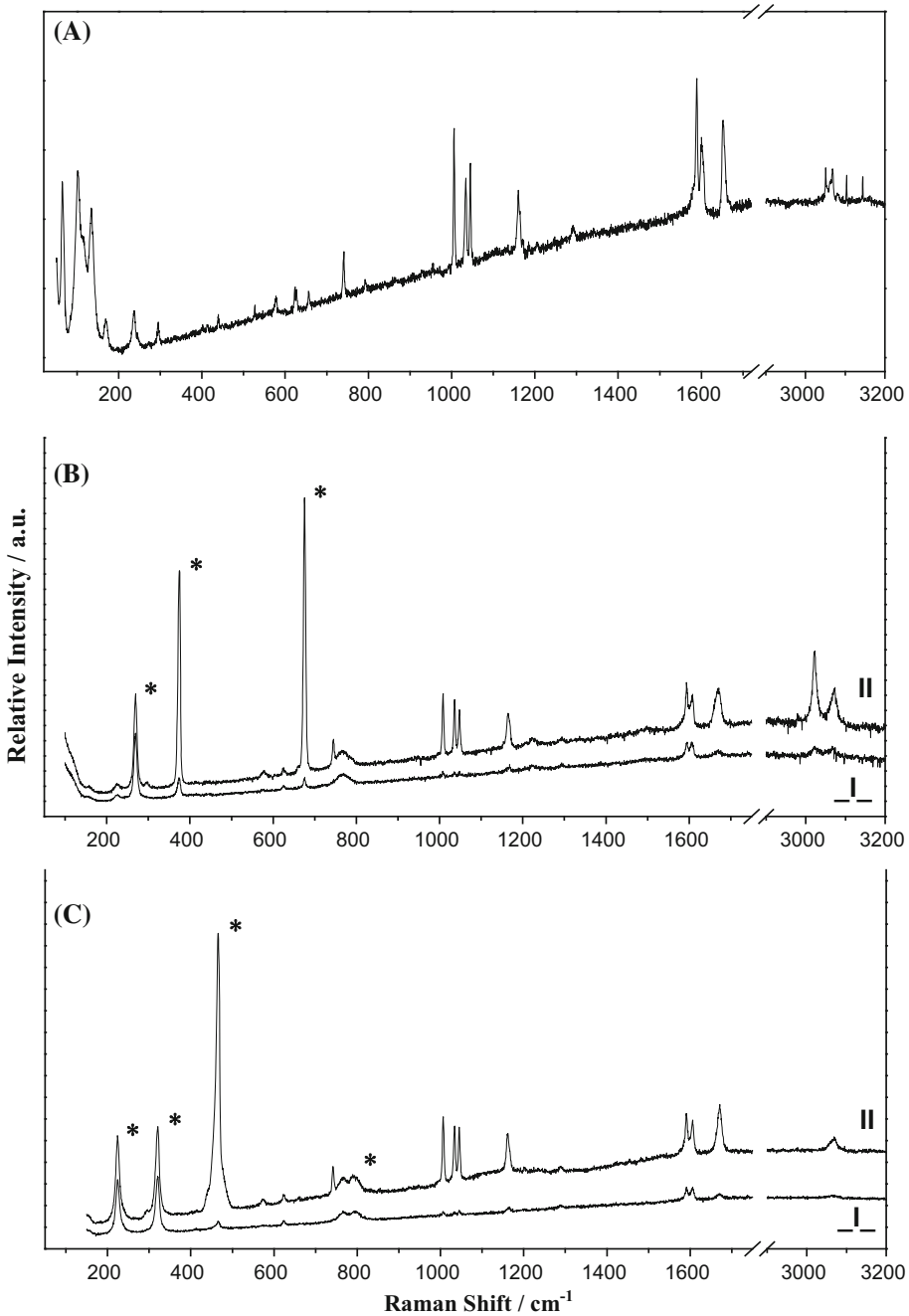

Fig. 2 Raman spectra of 3-BOP with excitation wavelength 514.5 nm; (A) for solid substance; (B) parallel and perpendicular components in $CHCl_3$ solution and (C) parallel and perpendicular components in CCl_4 solution. Asterisks indicate respective solvent bands

spectra of the molecule, but they did not make the complete assignment. So a thorough examination of the infrared and polarized Raman spectra of the molecule has been carried out and the normal modes have been assigned with the aid of QCC. A good assignment is necessary for analyzing the REPs of different normal modes, to be discussed later on, to get insight into the excited state properties of the molecule.

No difficulty arises in assigning the six ring angle bending modes (α_{ccc}) of the two rings and they are assigned unambiguously by examining the PEDs. Out of the CC and CC/CN stretching modes of the two rings, those derived from the normal modes 19(a,b) and 8(a,b) of benzene are assigned very easily in the respective regions (1400-1500) and (1500-1600) cm^{-1}. But some difficulties are encountered in assigning the ring breathing modes. In order to solve the problem, we had to take help of the animated views of the normal modes along with the PEDs. Thus these modes of the phenyl and the pyridyl rings are respectively assigned to the band around 910 (for which no experimental band is observed) and the strongly polarized Raman band around 1032 cm^{-1}. For the assignment of the

Table 3 Vibrational assignments of Raman and infrared bands (cm^{-1}) of 3-BOP

RAMAN			IR	CIS[a]	PED following CIS configuration	Assignment	TRANS[b]	PED following TRANS configuration	Assignment
Solid	In $CHCl_3$	In CCl_4							
				41	φ_{C7C8}(II)49, φ_{C6C7}(I)45.	CCx torsion (II)	43	φ_{C7C8}(II)50, φ_{C6C7}(I)44.	CCx torsion (II)
				59	φ_{C6C7}(I)26, φ_{C7C8}(II)23, α_{C6C7C8}(I)20, β_{C6C7}(I)11, β_{C7C8}(II)10.	CCx torsion (I)	60	φ_{C6C7}(I)31, α_{C6C7C8}(I)20, φ_{C7C8}(II)19, β_{C6C7}(I)12, β_{C7C8}(II)10.	CCx torsion (I)
				91	δ_{C6C7C8}25, γ_{C6C7}(I)17, γ_{C7C8}(II)14, φ_{CC}(I)10, φ_{CC}(II)10.	CC_X wag (sym)	91	δ_{C6C7C8}23, γ_{C6C7}(I)14, γ_{C7C8}(II)14, φ_{CC}(I)12, φ_{CC}(II)10.	CC_X wag (sym)
163 (m)	152 (w) D			134	γ_{C7C8}(II)19, γ_{C6C7}(I)15, φ_{C7C8}(II)15, φ_{C6C7}(I)15, γ_{C7O23}10, φ_{CC}(II)7, φ_{CC}(I)5.	CC_X wag (asym)	133	γ_{C7C8}(II)17, γ_{C6C7}(I)16, φ_{C7C8}(II)16, φ_{C6C7}(I)16, γ_{C7O23}9, φ_{CC}(II)6, φ_{CC}(I)6.	CC_X wag (asym)
230 (m)	221 (w) D			205	φ_{CC}(II)17, φ_{CC}(II)14, β_{C6C7}(I)13, β_{C7C8}(II)11, γ_{C7C8}(II)9, γ_{C6C7}(I)8.	CCx bend (sym)	208	φ_{CC}(II)15, φ_{CC}(I)15, β_{C6C7}(I)13, β_{C7C8}(II)10, γ_{C7C8}(II)10, γ_{C6C7}(I)9.	CCx bend (sym)
239 (sh)	242 (sh)	237 (sh)		227	β_{C6C7}(I)37, β_{C7C8}(II)34, δ_{C7O23}5, φ_{CC}(I)5.	CCx bend (asym)	228	β_{C7C8}(II)37, β_{C6C7}(I)35.	CCx bend (asym)
287 (m)	288 (w) P	290 (vw) P		278	ν_{C6C7}(I)19, ν_{C7C8}(II)16, β_{C7C8}(II)12, α_{CCC}(II)11, α_{CCC}(I)11, δ_{C6C7C8}7, β_{C6C7}(I)6.	CCx stretch (sym)	282	ν_{C6C7}(I)18, ν_{C7C8}(II)18, α_{CCC}(II)12, α_{CCC}(I)10, β_{C6C7}(I)10, β_{C7C8}(II)8, δ_{C6C7C8}6.	CCx stretch (sym)
				361	φ_{CC}(I)31, δ_{C7O23}19, φ_{CC}(II)13, γ_{C6C7}(I)10.	CxO bend	364	φ_{CC}(I)24, δ_{C7O23}21, φ_{CC}(II)13, γ_{C6C7}(I)10.	CxO bend
393 (vw)		397 (vw)	400 (w)	394	φ_{CC}(I)62, φ_{CC}(II)11, γ_{C4H20}(I)6.	Ring torsion (I)	394	φ_{CC}(I)61, φ_{CC}(II)12, γ_{C2H21}(I)6.	Ring torsion (I)
407 (w)	407 (vw) D	406 (vw) D	410 (m)	408	φ_{CC}(II)74.	Ring torsion (II)	408	φ_{CC}(II)73, φ_{CC}(I)5.	Ring torsion (II)
431 (m)	433 (vvw)	432 (vvw)	433 (m)	429	φ_{CC}(I)53, γ_{C6C7}(I)19, α_{CCC}(II)5.	Ring torsion (I)	431	φ_{CC}(I)43, γ_{C6C7}(I)16, φ_{CC}(II)8, α_{CCC}(II)5.	Ring torsion (I)
441 (vw)		439 (vvw)	440 (m)	438	φ_{CC}(II)54, γ_{C7C8}(II)22.	Ring torsion (II)	437	φ_{CC}(II)46, γ_{C7C8}(II)19, φ_{CC}(I)6.	Ring torsion (II)
520 (w)						239 + 287			239 + 287

Table 3 continued

RAMAN			IR	CIS[a]	PED following CIS configuration	Assignment	TRANS[b]	PED following TRANS configuration	Assignment
Solid	In $CHCl_3$	In CCl_4							
571 (m)	570 (w) P	568 (w) P	571 (m)	562	$\delta_{C6C7C8}30$, $\varphi_{CC}(II)12$, $\alpha_{CCC}(II)6$, $\gamma_{C6C7}(I)6$, $\varphi_{CC}(I)6$.	CCxC bend	558	$\delta_{C6C7C8}31$, $\varphi_{CC}(II)13$, $\alpha_{CCC}(II)6$, $\alpha_{CCC}(I)5$, $\gamma_{C6C7}(I)5$, $\varphi_{CC}(I)5$.	CCxC bend
				614	$\alpha_{CCC}(I)66$, $\alpha_{CCC}(II)19$.	Ring CCC bend (I)	612	$\alpha_{CCC}(I)45$, $\alpha_{CCC}(II)35$.	Ring CCC bend (I)
620 (m)	616 (w) D	619 (w) D	620 (m)	616	$\alpha_{CCC}(II)60$, $\alpha_{CCC}(I)19$.	Ring CCC bend (II)	615	$\alpha_{CCC}(II)51$, $\alpha_{CCC}(I)30$.	Ring CCC bend (II)
649 (m)	653 (vw)	653 (w) P	654 (s)	650	$\alpha_{CCC}(II)32$, $\alpha_{CCC}(I)22$, $\delta_{C7O23}15$, $\varphi_{CC}(II)10$.	Ring CCC bend (II)	651	$\alpha_{CCC}(II)31$, $\alpha_{CCC}(I)21$, $\delta_{C7O23}18$, $\varphi_{CC}(II)10$.	Ring CCC bend (II)
			691 (vs)	688	$\varphi_{CC}(II)65$, $\gamma_{C10H17}(II)7$, $\gamma_{C12H15}(II)7$, $\varphi_{CC}(I)7$.	Ring torsion (II)	688	$\varphi_{CC}(II)65$, $\gamma_{C10H17}(II)8$, $\gamma_{C12H15}(II)8$, $\varphi_{CC}(I)6$.	Ring torsion (II)
			706 (vvs)	700	$\varphi_{CC}(I)30$, $\gamma_{C10H17}(II)13$, $\gamma_{C12H15}(II)13$, $\gamma_{C7O23}10$, $\gamma_{C11H16}(II)10$, $\gamma_{C13H14}(II)5$.	CH wag (II)	701	$\varphi_{CC}(I)26$, $\gamma_{C10H17}(II)13$, $\gamma_{C12H15}(II)13$, $\gamma_{C7O23}12$, $\gamma_{C11H16}(II)11$, $\gamma_{C13H14}(II)6$, $\gamma_{C9H18}(II)6$.	CH wag (II)
			715 (s, sh)	711	$\varphi_{CC}(I)44$, $\gamma_{C4H20}(I)20$, $\gamma_{C6C7}(I)8$.	Ring torsion (I)	710	$\varphi_{CC}(I)48$, $\gamma_{C2H21}(I)20$, $\gamma_{C6C7}(I)8$.	Ring torsion (I)
733 (s)	736 (m) P	735 (m) P	735 (m, sh)	727	$\alpha_{CCC}(I)32$, $\alpha_{CCC}(II)15$, $\nu_{C7C8}(II)9$, $\nu_{C6C7}(I)9$, $\nu_{C5C6}(I)6$.	Ring CCC bend (I)	728	$\alpha_{CCC}(I)32$, $\alpha_{CCC}(II)14$, $\nu_{C7C8}(II)9$, $\nu_{C6C7}(I)8$.	Ring CCC bend (I)
785 (w)			785 (vs)	780	$\varphi_{CC}(II)19$, $\gamma_{C11H16}(II)13$, $\gamma_{C7C8}(II)12$, $\gamma_{C1H19}(I)8$, $\varphi_{CC}(I)8$, $\gamma_{C4H20}(I)8$, $\gamma_{C7O23}6$, $\gamma_{C3H21}(I)6$.	CH wag (I)	780	$\varphi_{CC}(II)21$, $\gamma_{C11H16}(II)13$, $\gamma_{C7C8}(II)13$, $\gamma_{C7O23}7$, $\varphi_{CC}(I)7$, $\gamma_{C1H22}(I)7$, $\gamma_{C2H21}(I)6$, $\gamma_{C3H20}(I)5$.	CH wag (I)
			833 (vs)	821	$\varphi_{CC}(I)17$, $\gamma_{C4H20}(I)16$, $\gamma_{C7O23}15$, $\gamma_{C6C7}(I)11$, $\gamma_{C3H21}(I)11$, $\gamma_{C5H19}(I)10$.	C_XO wag	829	$\varphi_{CC}(I)19$, $\gamma_{C2H21}(I)17$, $\gamma_{C7O23}14$, $\gamma_{C6C7}(I)12$, $\gamma_{C3H20}(I)12$, $\gamma_{C1H22}(I)10$.	C_XO wag
			856 (vvw)	842	$\gamma_{C12H15}(II)28$, $\gamma_{C10H17}(II)24$, $\gamma_{C13H14}(II)23$, $\gamma_{C9H18}(II)21$.	CH wag (II)	841	$\gamma_{C12H15}(II)28$, $\gamma_{C10H17}(II)25$, $\gamma_{C13H14}(II)23$, $\gamma_{C9H18}(II)21$.	CH wag (II)

Table 3 continued

RAMAN			IR	CIS[a]	PED following CIS configuration	Assignment	TRANS[b]	PED following TRANS configuration	Assignment
Solid	In $CHCl_3$	In CCl_4							
				910	δ_{C7O23}19, α_{CCC}(I)10, ν_{C8C13}(II)9, α_{CCC}(II)8, ν_{C1C6}(I)8, γ_{C9H18}(II)5.	CC stretch (II)	912	δ_{C7O23}17, ν_{C8C13}(II)9, α_{CCC}(I)8, α_{CCC}(II)8, ν_{C1C6}(I)8, γ_{C9H18}(II)8, γ_{C11H16}(II)6, γ_{C13H14}(II)6.	CC stretch (II)
922 (w)			923 (s)	930	γ_{C9H18}(II)25, γ_{C11H16}(II)17, γ_{C13H14}(II)15, γ_{C1H22}(I)14.	CH wag (II)	932	γ_{C9H18}(II)27, γ_{C11H16}(II)19, γ_{C13H14}(II)16.	CH wag (II)
935 (w)			937 (s)	938	γ_{C1H22}(I)28, γ_{C3H21}(I)25, γ_{C5H19}(I)10, φ_{CC}(I)8, γ_{C9H18}(II)6, γ_{C11H16}(II)5.	CH wag (I)	936	γ_{C5H19}(I)47, γ_{C3H20}(I)20, φ_{CC}(I)9, γ_{C1H22}(I)7, γ_{C2H21}(I)5.	CH wag (I)
947 (w)			950 (s)	960	γ_{C5H19}(I)30, γ_{C1H22}(I)25, φ_{CC}(I)8, γ_{C4H20}(I)7, γ_{C3H21}(I)7.	CH wag (I)	963	γ_{C3H20}(I)19, γ_{C1H22}(I)16, γ_{C5H19}(I)16, γ_{C10H17}(II)11, γ_{C9H18}(II)10, γ_{C13H14}(II)9, γ_{C12H15}(II)6.	CH wag (I)
			978 (w)	967	γ_{C10H17}(II)24, γ_{C13H14}(II)21, γ_{C9H18}(II)20, γ_{C12H15}(II)10, φ_{CC}(II)6.	CH wag (II)	968	γ_{C10H17}(II)16, γ_{C13H14}(II)16, γ_{C5H19}(I)14, γ_{C9H18}(II)14, γ_{C1H22}(I)10, γ_{C12H15}(II)8, γ_{C3H20}(I)7.	CH wag (II)
	985 (w)			983	γ_{C4H20}(I)31, γ_{C3H21}(I)28, γ_{C5H19}(I)17, γ_{C1H22}(I)11.	CH wag (I)	986	γ_{C2H21}(I)33, γ_{C1H22}(I)26, γ_{C3H20}(I)19, φ_{CC}(I)7.	CH wag (I)
993 (w)	994 (sh) P	989 (w) P		985	γ_{C12H15}(II)26, γ_{C11H16}(II)24, φ_{CC}(II)15, γ_{C10H17}(II)13, γ_{C13H14}(II)12.	CH wag (II)	984	γ_{C12H15}(II)25, γ_{C11H16}(II)25, φ_{CC}(II)15, γ_{C10H17}(II)14, γ_{C13H14}(II)11.	CH wag (II)
				988	α_{CCC}(II)54, ν_{C8C13}(II)7, ν_{C8C9}(II)7, ν_{C9C10}(II)5.	Ring CCC bend (II)	988	α_{CCC}(II)57, ν_{C8C13}(II)7, ν_{C8C9}(II)7, ν_{C9C10}(II)5.	Ring CCC bend (II)
998 (vs)	1000 (vs) P	1001 (vs) P	999 (sh)	1012	α_{CCC}(I)62, ν_{C5C6}(I)11, ν_{C1C6}(I)10.	Ring CCC bend (I)	1011	α_{CCC}(I)65, ν_{C1C6}(I)12, ν_{C5C6}(I)9.	Ring CCC bend (I)
1027 (s)	1028 (vs) P	1028 (vs) P	1026 (m)	1019	ν_{C11C12}(II)26, ν_{C10C11}(II)24, α_{CCC}(II)10, β_{C12H15}(II)6, β_{C10H17} (II)6.	CH bend (II)	1019	ν_{C11C12}(II)26, ν_{C10C11}(II)25, α_{CCC}(II)10, β_{C12H15}(II)6, β_{C10H17} (II)6.	CH bend (II)

Table 3 continued

RAMAN			IR	CIS[a]	PED following CIS configuration	Assignment	TRANS[b]	PED following TRANS configuration	Assignment
Solid	In $CHCl_3$	In CCl_4							
1038 (vs)	1039 (vs) P	1039 (vs) P	1038 (m)	1032	ν_{C3C4}(I)36, ν_{C3N2}(I)20, ν_{C4C5}(I)11, β_{C4H20}(I)11.	CC/CN stretch (I)	1031	ν_{C2C3}(I)39, ν_{C3N4}(I)17, β_{C2H21}(I)11, ν_{C1C2}(I)8.	CC/CN stretch (I)
			1078 (m)	1074	ν_{C9C10}(II)21, ν_{C12C13}(II)17, β_{C13H14}(II)14, β_{C11H16}(II)12, β_{C9H18}(II)9, ν_{C10C11}(II)6, ν_{C11C12}(II)6.	CH bend (II)	1073	ν_{C9C10}(II)21, ν_{C12C13}(II)17, β_{C13H14}(II)14, β_{C11H16}(II)13, β_{C9H18}(II)9, ν_{C10C11}(II)7, ν_{C11C12}(II)5.	CH bend (II)
1099 (vw)			1101 (m)	1108	β_{C5H19}(I)29, ν_{C4C5}(I)21, β_{C4H20}(I)18, ν_{C1N2}(I)11.	CH bend (I)	1102	β_{C1H22}(I)34, ν_{C1C2}(I)18, β_{C2H21}(I)16, ν_{C5N4}(I)13.	CH bend (I)
			1124 (m)	1137	ν_{C7C8}(II)15, ν_{C6C7}(I)10, α_{CCC}(II)10, β_{C4H20}(I)9, α_{CCC}(I)9, ν_{C4C5}(II)8, ν_{C8C13}(I)7, ν_{C1C6}(II)7, β_{C13H14}(II)6.	CH bend (I)	1138	ν_{C7C8}(II)16, ν_{C6C7}(I)11, α_{CCC}(II)10, α_{CCC}(I)9, β_{C2H21}(I)9, ν_{C8C13}(II)7, ν_{C1C6}(I)6, β_{C13H14}(II)6.	CH bend (I)
1153 (vs)	1157 (vs) P	1155 (vs) P	1153 (s)	1150	β_{C11H16}(II)36, β_{C12H15}(II)22, β_{C10H17}(II)16, ν_{C10C11}(II)8, ν_{C11C12}(II)8.	CH bend (II)	1150	β_{C11H16}(II)36, β_{C12H15}(II)22, β_{C10H17}(II)15, ν_{C10C11}(II)8, ν_{C11C12}(II)8.	CH bend (II)
1164 (sh)	1163 (sh) P	1164 (sh) P	1164 (w)	1168	β_{C10H17}(II)24, β_{C9H18}(II)17, β_{C13H14}(II)17, β_{C12H15}(II)16, ν_{C9C10}(II)10, ν_{C12C13}(II)6.	CH bend (II)	1167	β_{C10H17}(II)25, β_{C9H18}(II)18, β_{C13H14}(II)17, β_{C12H15}(II)16, ν_{C9C10}(II)10, ν_{C12C13}(II)5.	CH bend (II)
1199 (w)			1200 (m)	1190	β_{C3H21}(I)20, ν_{C2N3}(I)19, β_{C1H22}(I)13, ν_{C3C4}(I)11, β_{C4H20}(I)11, β_{C5H19}(I)6, ν_{C5C6}(I)6.	CH bend (I)	1188	β_{C3H20}(I)22, ν_{C3N4}(I)19, β_{C2H21}(I)13, ν_{C2C3}(I)11, ν_{C5N4}(I)8, β_{C1H22}(I)7, β_{C5H19}(I)7.	CH bend (I)
1237 (w)		1233 (vw)	1239 (m)	1247	ν_{C1N2}(I)21, ν_{C2C3}(I)17, ν_{C1C6}(I)14, ν_{C3C4}(I)10, ν_{C4C5}(I)9, ν_{C5C6}(I)8.	CC/CN stretch (I)	1243	ν_{C5C6}(I)19, ν_{C5N4}(I)17, ν_{C3N4}(I)14, ν_{C1C2}(I)11, ν_{C2C3}(I)7, ν_{C1C6}(I)7, ν_{C6C7}(I)6.	CC/CN stretch (I)
		1260 (w)	1261 (sh)	1252	ν_{C6C7}(I)22, ν_{C7C8}(II)19, ν_{C5C6}(I)11, ν_{C1N2}(I)10.	CC_X stretch (asym)	1260	ν_{C6C7}(I)16, ν_{C7C8}(II)16, ν_{C5N4}(I)13, ν_{C3N4}(I)9, ν_{C1C6}(I)7, ν_{C2C3}(I)6, δ_{C7O23}6.	CC_X stretch (asym)

Table 3 continued

RAMAN			IR	CIS[a]	PED following CIS configuration	Assignment	TRANS[b]	PED following TRANS configuration	Assignment
Solid	In $CHCl_3$	In CCl_4							
1288 (m)	1287 (vw)	1287 (w)	1286 (vs)	1295	ν_{C8C13}(II)18, ν_{C8C9}(II)18, ν_{C10C11}(II)10, ν_{C11C12}(II)10, ν_{C9C10}(II)9, β_{C12H15}(II)8, ν_{C12C13}(II)7, β_{C10H17}(II)6.	CC stretch (II)	1295	ν_{C8C13}(II)18, ν_{C8C9}(II)18, ν_{C10C11}(II)10, ν_{C11C12}(II)10, ν_{C9C10}(II)9, β_{C12H15}(II)8, ν_{C12C13}(II)7, β_{C10H17}(II)6.	CC stretch (II)
			1311 (s)	1315	β_{C9H18}(II)24, β_{C13H14}(II)24, ν_{C12C13}(II)11, β_{C11H16}(II)10, ν_{C9C10}(II)9, ν_{C10C11}(II)7, ν_{C11C12}(II)5.	CH bend (II)	1314	β_{C9H18}(II)24, β_{C13H14}(II)23, ν_{C12C13}(II)11, β_{C11H16}(II)10, ν_{C9C10}(II)8, ν_{C10C11}(II)7, ν_{C11C12}(II)5.	CH bend (II)
			1320 (s)	1319	β_{C1H22}(I)43, β_{C5H19}(I)24, β_{C3H21}(I)16.	CH bend (I)	1321	β_{C5H19}(I)40, β_{C1H22}(I)25, β_{C3H20}(I)12, β_{C2H21}(I)9.	CH bend (I)
			1334 (s)			620 + 715/			
654 + 691			620 + 715/ 654 + 691						
			1399 (sh)	1406	β_{C3H21}(I)30, ν_{C1C6}(I)17, ν_{C1N2}(I)15, β_{C5H19}(I)9, β_{C6C7}(I)5.	CC stretch (I)	1403	β_{C3H20}(I)38, ν_{C5C6}(I)15, ν_{C5N4}(I)14, β_{C1H22}(I)6, ν_{C2C3}(I)6, ν_{C1C6}(I)6.	CC stretch (I)
			1422 (s)	1435	β_{C11H16}(II)26, β_{C10H17}(II)15, ν_{C9C10}(II)13, ν_{C12C13}(II)12, β_{C12H15}(II)12, ν_{C8C13}(II)5, ν_{C8C9}(II)5.	CC stretch (II)	1434	β_{C11H16}(II)26, β_{C10H17}(II)15, ν_{C9C10}(II)13, ν_{C12C13}(II)12, β_{C12H15}(II)12, ν_{C8C13}(II)5, ν_{C8C9}(II)5.	CC stretch (II)
1450 (w)			1447 (s)	1458	β_{C4H20}(I)26, β_{C1H20}(I)20, ν_{C3N2}(I)12, β_{C3H21}(II)11, ν_{C4C5}(I)9, ν_{C5C6}(I)7.	CC stretch (I)	1461	β_{C2H21}(I)24, β_{C5H19}(I)23, ν_{C3N4}(I)9, ν_{C1C6}(I)9, ν_{C1C2}(I)7, β_{C3H20}(II)6.	CC stretch (I)
1480 (w)			1473 (m)	1477	β_{C12H15}(II)17, β_{C9H18}(II)15, β_{C10H17}(II)15, β_{C13H14}(II)14, ν_{C11C12}(II)10, ν_{C8C13}(II)9, ν_{C8C9}(II)7, ν_{C10C11}(II)7.	CC stretch (II)	1476	β_{C12H15}(II)16, β_{C9H18}(II)15, β_{C10H17}(II)15, β_{C13H14}(II)13, ν_{C11C12}(II)9, ν_{C8C13}(II)9, ν_{C8C9}(II)7, ν_{C10C11}(II)7.	CC stretch (II)
			1517 (m, sh)			691 + 833/ 733 + 785			691 + 833/ 733 + 785

Table 3 continued

RAMAN			IR	CIS[a]	PED following CIS configuration	Assignment	TRANS[b]	PED following TRANS configuration	Assignment
Solid	In $CHCl_3$	In CCl_4							
				1558	ν_{C3C4}(I)24, ν_{C5C6}(I)15, ν_{C3N2}(I)13, ν_{C1C6}(I)13, β_{C3H21}(I)12, α_{CCC}(I)8.	CC/CN stretch (I)	1556	ν_{C2C3}(I)20, ν_{C1C6}(I)17, ν_{C3N4}(I)16, ν_{C5C6}(I)13, β_{C3H20}(I)13, α_{CCC}(I)8.	CC/CN stretch (I)
1573 (w)	1578 (sh)	1573 (sh)	1577 (sh)	1572	ν_{C10C11}(II)20, ν_{C11C12}(II)17, ν_{C8C9}(II)13, ν_{C8C13}(II)13, β_{C11H16}(II)10, α_{CCC}(II)8.	CC stretch (II)	1571	ν_{C10C11}(II)21, ν_{C11C12}(II)17, ν_{C8C9}(II)14, ν_{C8C13}(II)13, β_{C11H16}(II)11, α_{CCC}(II)9.	CC stretch (II)
1582 (vvs)	1585 (vs) P	1582 (s) P	1583 (vs)	1577	ν_{C4C5}(I)24, ν_{C1N2}(I)15, ν_{C5C6}(I)12, α_{CCC}(I)10, β_{C5H19}(I)9, β_{C1H22}(I)7.	CC/CN stretch (I)	1578	ν_{C1C2}(I)28, ν_{C5N4}(I)14, α_{CCC}(I)10, β_{C1H22}(I)8, ν_{C1C6}(I)8, β_{C5H19}(I)7, ν_{C5C6}(I)7.	CC/CN stretch (I)
1592 (vvs)	1599 (vs) P	1598 (vs) P	1596 (s)	1592	ν_{C12C13}(II)23, ν_{C9C10}(II)20, α_{CCC}(II)10, ν_{C8C9}(II)7, β_{C9H18}(II)6, β_{C13H14}(II)6, ν_{C8C13}(II)5, ν_{C11C12}(II)5, β_{C12H15}(II)5.	CC stretch (II)	1591	ν_{C12C13}(II)23, ν_{C9C10}(II)20, α_{CCC}(II)10, ν_{C8C9}(II)7, β_{C9H18}(II)6, β_{C13H14}(II)6, ν_{C8C13}(II)5, ν_{C11C12}(II)5, β_{C12H15}(II)5.	CC stretch (II)
1615 (vvw)			1616 (w, sh)			785 + 833			785 + 833
1644 (vvs)	1661 (vs) P	1665 (vs) P	1646 (vvs)	1663	ν_{C7O23}79, δ_{C6C7C8}7.	C_XO stretch	1659	ν_{C7O23}79, δ_{C6C7C8}8.	C_XO stretch
3033 (vw)	3033 (vw)	3032 (w)	3033 (sh)	3032	ν_{C3H21}(I)93, ν_{C4H20}(I)6.	CH stretch (I)	3031	ν_{C3H20}(I)93, ν_{C2H21}(I)5.	CH stretch (I)
3047 (sh)	3043 (sh) P			3047	ν_{C11H16}(II)43, ν_{C10H17}(II)30, ν_{C12H15}(II)21.	CH stretch (II)	3046	ν_{C11H16}(II)34, ν_{C10H17}(II)23, ν_{C5H19}(I)20, ν_{C12H15}(II)17.	CH stretch (II)
3051 (m)	3050 (w) P			3055	ν_{C1H22}(I)96.	CH stretch (I)	3047	ν_{C5H19}(I)77, ν_{C11H16}(II)11, ν_{C12H15}(II)6.	CH stretch (I)
3056 (sh)	3057 (sh) P	3056 (sh) P	3057 (m)	3056	ν_{C12H15}(II)43, ν_{C10H17}(II)38, ν_{C9H18}(II)11.	CH stretch (II)	3057	ν_{C12H15}(II)44, ν_{C10H17}(II)42, ν_{C9H18}(II)8.	CH stretch (II)
3062 (m)	3062 (s) P			3061	ν_{C5H19}(I)51, ν_{C4H20}(I)37.	CH stretch (I)	3064	ν_{C2H21}(I)68, ν_{C1H22}(I)26.	CH stretch (I)
3069 (m)	3072 (sh) P	3069 (m) P		3066	ν_{C11H16}(II)43, ν_{C9H18}(II)22, ν_{C12H15}(II)18, ν_{C13H14}(II)9.	CH stretch (II)	3067	ν_{C11H16}(II)46, ν_{C9H18}(II)19, ν_{C12H15}(II)17, ν_{C13H14}(II)9, ν_{C10H17}(II)8.	CH stretch (II)
3077 (sh)				3074	ν_{C9H18}(II)30, ν_{C4H20}(I)27, ν_{C5H19}(I)17, ν_{C10H17}(II)14, ν_{C11H16}(II)5.	CH stretch (II)	3076	ν_{C9H18}(II)65, ν_{C10H17}(II)20, ν_{C13H14}(II)9.	CH stretch (II)

Table 3 continued

RAMAN			IR	CIS[a]	PED following CIS configuration	Assignment	TRANS[b]	PED following TRANS configuration	Assignment
Solid	In $CHCl_3$	In CCl_4							
	3080 (sh) P	3079 (sh)	3080 (m)	3076	ν_{C9H18}(II)30, ν_{C5H19}(I)28, ν_{C4H20}(I)24, ν_{C10H17}(II)9.	CH stretch (I)	3079	ν_{C1H22}(I)69, ν_{C2H21}(I)24.	CH stretch (I)
				3079	ν_{C13H14}(II)76, ν_{C12H15}(II)15.	CH stretch (II)	3080	ν_{C13H14}(II)71, ν_{C12H15}(II)14.	CH stretch (II)

ν, stretching; α, in-plane ring bending; β, in-plane angle bending; δ, in-plane substitute bending; γ, wagging; ϕ, torsion

C_X, carbon atom of carbonyl group

[a] Scaling factor for CIS is 0.9623. Percentage error in wavenumber calculation is 1.02% (8.05 cm^{-1})

[b] Scaling factor for TRANS is 0.9622. Percentage error in wavenumber calculation is 0.98% (7.94 cm^{-1})

former one, we had to depend completely on the theoretical calculation and animated view of the said normal mode. Mautner et al. [15] assigned the two strong and polarized Raman bands at 1000 and 1028 cm^{-1} to the breathing vibrations of the two rings. But present calculations have confirmed them to be rather different, the angle bending vibration [α_{CCC}(I)] of the pyridyl and CH bending vibrations of the phenyl [β_{CH}(II)] rings respectively. The respective Kekule modes of the two rings are assigned easily to the weak and medium strong Raman bands at 1237 and 1288 cm^{-1} (corresponding to the medium and strong infrared counterparts at 1239 and 1286 cm^{-1} respectively). The CH bending modes (including those derived from mode number 3, lying around 1300 cm^{-1}) are assigned without much difficulty and they are in compliance with the previous works. One thing is to be pointed out in this regard. The PEDs of the modes near 1000 cm^{-1} are mixed up very intricately, so care has been taken to assign them properly.

In regard to the assignments of the substituent sensitive modes, we have revised some of those made by Chaudhury et al. [16]. The polarized Raman vibration around 570 cm^{-1} was assigned by them to the in-plane bending vibrations of the carbonyl group, but our calculations have shown that this is the angle bending mode [$\delta(CC_XC)$], suffix X being the carbonyl carbon. The in-plane bending vibration [β(C=O)] has been assigned to the theoretical value (around 364 cm^{-1}) for which no Raman or infrared wave number is observed. Two weak Raman bands at 221 and 242 cm^{-1} are respectively assigned to the CC_X bending vibrations of the two rings I and II. Two important findings have been made by us. The polarized Raman band at 288 cm^{-1} has been assigned to stretching vibration [ν_{CCx}(I)] of the pyridyl ring and the corresponding one for the phenyl ring to the wavenumber 1260 cm^{-1}. Such a low value (288 cm^{-1}) is very unusual for a CC_X stretching vibration. But not only PED but animated view of the said mode compelled us to make this assignment. However such kind of observation has been made in the isomer (2-BOP) [8]. In a similar way, the out of plane bending vibration [$\gamma(C_XO)$] has been assigned to a quiet higher value, a strong infrared band at 833 cm^{-1}. But similar observation was made in the case of the isomer (2-BOP) [8]. In regard to the C=O stretching frequency, the magnitude (about 1663 cm^{-1}) is more or less same with those of the other two isomers, but is less than that (1685 cm^{-1}) of 2,2′-DPK [7]. This is in compliance with their respective C=O bond lengths, because $r_{C=O}$ is about 1.211 Å for 2,2′-DPK [7], whereas it lies in the range (1.218 – 1.221 Å) for the three isomers of BOP [8, 9].

Another point is to be noted in this respect. According to the observed spectra and theoretical calculations, it seems that both the isomers, CIS and TRANS, are present in the sample. Their relative population can be estimated from the ratio of the sum of the integrated intensities of the assigned experimental bands representing vibrational signatures of CIS and TRANS forms of the molecule to those of the theoretically predicted sums of absolute intensities A^{CIS} and A^{TRANS} of the respective bands i.e.

$$\frac{[CIS]}{[TRANS]} = \frac{\sum I^{CIS} \sum A^{TRANS}}{\sum I^{TRANS} \sum A^{CIS}}$$

Thus it is found that 51% of the TRANS and 49% of the CIS configurations are prevalent.

The potential energy profile for the internal rotation around the C_6C_7 bond, is shown in Fig. 3. The predicted energy barrier, measured from the bottom of the potential well of the TRANS and CIS structures, is found to be 12.91 kJ/mol and 10.68 kJ/mol for the two respective isomers. When the zero-point energy of the said vibration (CCx torsion) is taken into account, the respective barrier heights become 12.55 kJ/mol and 10.32 kJ/mol. In regard to the barrier heights of these magnitudes, it is not

unexpected for the stable existence of the molecule in both these forms.

The curve in between the two TRANS minima are asymmetric about the dihedral angle 180°, otherwise it appears to have a mirror symmetry. In the TRANS configuration at 220°, the H_{18}-atom of the phenyl ring is closest to the H_{19}-atom of the pyridyl ring (2.17 Å) making the molecule least stable. On the other hand the $H_{18}H_{19}$ bond distances are found to be 2.55/2.54 and 2.52/2.52 Å for the stable configurations of the pair of TRANS and CIS forms.

3.3. Electronic Spectra

The electronic absorption spectra of 3-BOP in cyclohexane (CHX), ethanol (EtOH) and methylcyclohexane (MCH) solutions at room temperature (300 K) are shown in Fig. 4 and the band positions are listed in Table 4. A weak band system is found to appear on the lower wavelength side of the spectra at higher concentration. In CHX solution, this band system exhibits a structure with the $0-0$ band and the band maximum observed at 380 nm (26,316 cm^{-1}) and 348 nm (28,736 cm^{-1}) respectively. The band structure is more or less identical in MCH environment with the $0-0$ band and the band maximum observed at 381 nm (26,247 cm^{-1}) and 349 nm (28,653 cm^{-1}) respectively. The spectra is analyzed in terms of a v' progression (originating from the level $v''=0$) of an excited state fundamental of wave number 1230 cm^{-1}. This wave number most probably corresponds to the C=O stretching vibration in the excited state (S_1), which is $n\pi^*$ in nature, found from the blue shift of the corresponding band in the alcohol solution (Table 4). Besides this band, a broad but strong band in EtOH solution is observed at 254 nm. The corresponding band in CHX/MCH solution is found at 250/249 nm. The red shift of this band in alcohol solution indicates that the nature of the transition is of the type $\pi \rightarrow \pi^*$. This band is assigned as the ^1L_a-band due to its position, intensity and lack of structure. The expected much weaker ^1L_b-band is found as a shoulder at 266 nm on the long wavelength wing of the ^1L_a-band in the CHX and EtOH solutions. A weak shoulder is observed around 241 nm in CHX/MCH solution. A prominent but medium strong band around 215 nm in CHX/MCH solution and another at 205 nm in EtOH solution are also observed.

To make an in depth study on the nature of the ultraviolet absorption spectra, the low energy electronic excited states of 3-BOP have been calculated at the B3LYP/6-311G(d,p) level using TD-DFT approach on the previously optimized ground state molecular geometry of the molecule. Transition energies and oscillator strengths for the CIS and TRANS isomers are listed in the Tables 5 and 6 respectively along with the description of absorptions expressed in terms of dominant one-electronic vertical transitions. The TD-DFT method predicts appreciable shifts of energies of singlet states in going from gas phase to different solvent phases (Tables 5, 6). From the computational work, it has been found that HOMO is the molecular orbital number 48 and the LUMO is the molecular orbital number 49. LUMO and other higher orbitals (LUMO + 1, LUMO + 2 and LUMO + 3) of the molecule are found to be of π-nature and spread over the both rings (Fig. 5). In the case of LUMO, the π-bonding orbital also encloses the carbonyl group, however the next three higher orbitals above LUMO do not dominantly

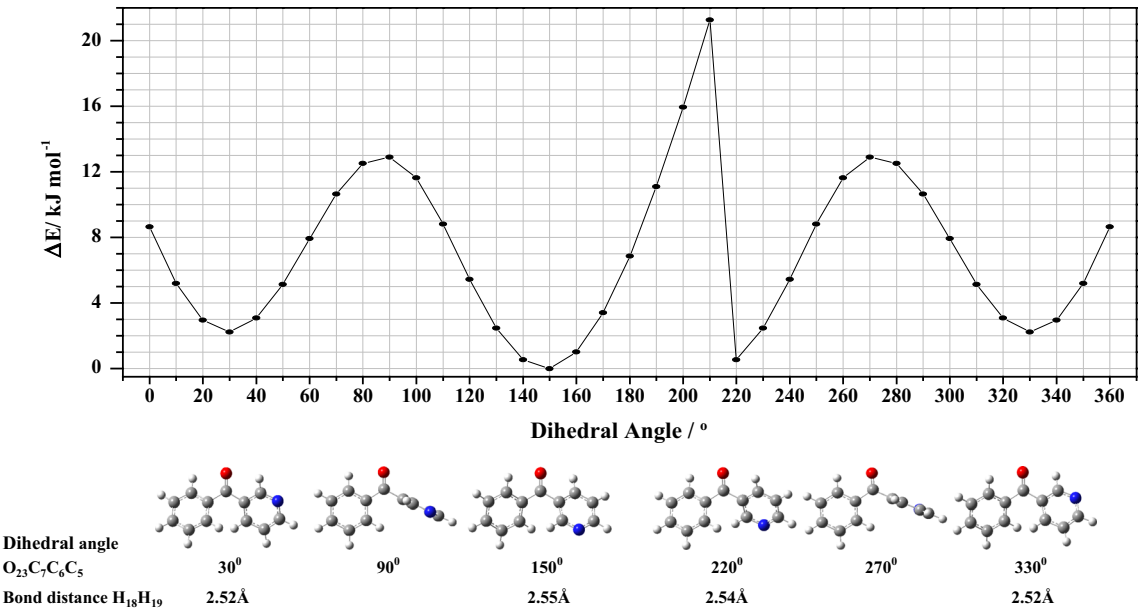

Fig. 3 Variation of energy of 3-BOP with dihedral angle ($O_{23}C_7C_6C_{1/5}$)

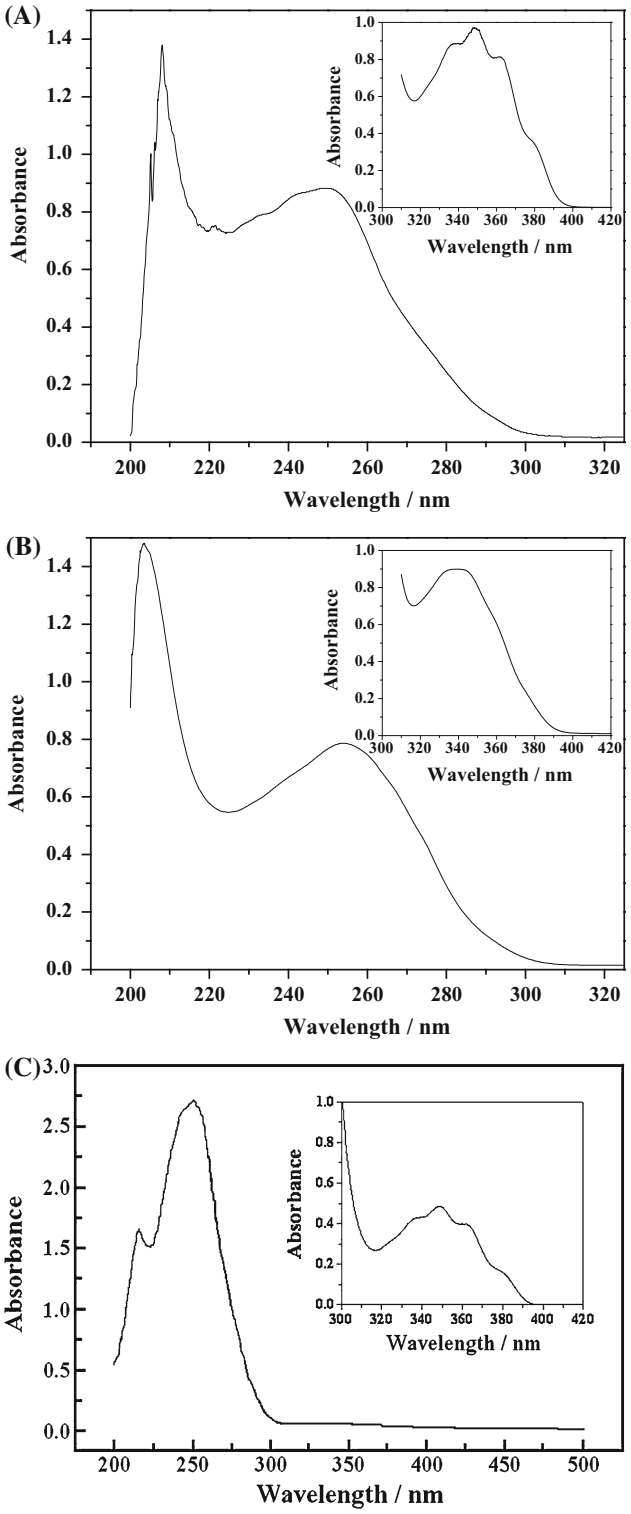

Fig. 4 Electronic absorptiom spectra of 3-BOP in (**a**) cyclohexane, (**b**) ethanol and (**c**) methyl cyclohexane solutions at concentration of the order of 10^{-5} M (approximately). (The *inset* spectra are taken at concentration of order of 10^{-3} M (approximately)

enclose the carbonyl group i.e. the atom positions, 7 and 23, have practically zero coefficients, but those of the atoms in the ring moieties have large coefficients in the molecular orbitals of the respective linear combinations of atomic orbitals (LCAO-MOs). On the other hand, HOMO, HOMO-4 and to some extent HOMO-1 and HOMO-2 have significant contributions both from the non-bonding orbitals and also from the π-clouds. The other orbital, HOMO-3 is found to exhibit π-orbital characteristics localized in the phenyl ring, whereas HOMO-5 (π-bonding orbital) is mainly confined on pyridyl ring.

The first transition (n → π^*) is calculated at the wavelength 350.39/350.95 nm in vacuum and at 347.24/347.50 and 337.05/337.28 nm of the TRANS/CIS isomers in the CHX and EtOH surroundings with very negligible oscillator strength. In all cases the vertical one electron excitation can be mainly described by the HOMO → LUMO transition. This band is corresponded with the weak band observed on the longer wavelength side of the electronic absorption spectra with the band maximum found at 348/349/343 nm in CHX/MCH/EtOH environments.

The next band, also n → π^* in nature, is calculated near 290 nm in vacuum where the leading transition is from (HOMO-1) → LUMO. But the transitions from (HOMO-3) → LUMO and (HOMO-4) → LUMO have also certain significant contributions. In CHX solvent the peak (at 288 nm) is slightly blue shifted and in EtOH environment it is further blue shifted to 284 nm in the trans isomer. In the CIS isomer, similar effect has also been observed. This band is correlated with the shoulder at 282/274 nm of the observed spectra in CHX/EtOH solutions.

The subsequent band system consists of four lines. Among them the first three lines (near 275, 263 and 253 nm in vacuum) exhibit prominent red shift in going from the non-polar to polar solvent with significant f-values. They are corresponded with the π → π^* transitions. The first one (associated mainly with 46 → 49 orbital transition) of this group is assigned as ^1L_b-band for comparatively low f-value. The other two bands (having higher f-values) appear to be the exciton split components of the ^1L_a-band where the chief transitions come from 44 → 49, 45 → 49, 46 → 49 and 47 → 49. Such kind of exciton splitting of the ^1L_a-band has also been observed in 4-BOP [9] and 2,2′-DPK [7]. Though all these bands could not be resolved in MCH solvent but appeared clearly in the observed spectra of the sample in CHX and EtOH solvents. The other band (near 235 nm in vacuum) having comparatively higher f-value shows practically no shift. The dominant orbital transitions are 43 → 49 and 45 → 50 for the trans isomer which redistribute the π-electronic cloud in the two rings and thus this is assigned to a

Table 4 Electronic absorption spectra of 3-BOP

In CHX solution at 300 K		In MCH solution at 300 K		In EtOH solution at 300 K	
Wavelength in nm (Wave number in cm^{-1})	Assignment	Wavelength in nm (Wave number in cm^{-1})	Assignment	Wavelength in nm (Wave number in cm^{-1})	Assignment
				205 (48780)	$^1G \rightarrow S_8$ ($\pi \rightarrow \pi^*$)
213 (46,948)	$^1G \rightarrow S_7$ ($\pi \rightarrow \pi^*$)	215 (46,512)	$^1G \rightarrow S_7$ ($\pi \rightarrow \pi^*$)		$^1G \rightarrow S_7$ ($\pi \rightarrow \pi^*$)
229 (43,688)	$^1G \rightarrow S_6$ ($n \rightarrow \pi^*$)			230 (43,478)	$^1G \rightarrow S_6$ ($\pi \rightarrow \pi^*$)
241 (41,494)	$^1G \rightarrow S_5$ ($\pi \rightarrow \pi^*$)	242 (41,322)	$^1G \rightarrow S_5$ ($\pi \rightarrow \pi^*$)	239 (41,841)	$^1G \rightarrow S_5$ ($\pi \rightarrow \pi^*$)
250 (40,000)	$^1G \rightarrow S_4$ ($\pi \rightarrow \pi^*$)	249 (40,161)	$^1G \rightarrow S_4$ ($\pi \rightarrow \pi^*$)	254 (39,370)	$^1G \rightarrow S_4$ ($\pi \rightarrow \pi^*$)
266 (37,594)	$^1G \rightarrow S_3$ ($\pi \rightarrow \pi^*$)			266 (37,594)	$^1G \rightarrow S_3$ ($\pi \rightarrow \pi^*$)
282 (35,461)	$^1G \rightarrow S_2$ ($n \rightarrow \pi^*$)			274 (36,496)	$^1G \rightarrow S_2$ ($n \rightarrow \pi^*$)
	$^1G \rightarrow S_1$ ($n \rightarrow \pi^*$) ▼		$^1G \rightarrow S_1$ ($n \rightarrow \pi^*$) ▼		$^1G \rightarrow S_1$ ($n \rightarrow \pi^*$) ▼
324 (30,864)	$0 + 4 \times 1230$	324 (30,864)	$0 + 4 \times 1230$		
336 (29,674)	$0 + 3 \times 1230$	336 (29,762)	$0 + 3 \times 1230$	334 (29,940)	$0 + 3 \times 1230$
348 (28,736)	$0 + 2 \times 1230$	349 (28,653)	$0 + 2 \times 1230$	343 (29,155)	$0 + 2 \times 1230$
363 (27,548)	$0 + 1230$	364 (27,473)	$0 + 1230$	357 (28,011)	$0 + 1230$
380 (26,316)	0–0	381 (26,247)	0–0	374 (26,738)	0–0

$\pi \rightarrow \pi^*$ band. For the CIS isomer, the corresponding band appear from the transitions dominated by $43 \rightarrow 49$, $47 \rightarrow 50$, $48 \rightarrow 50$, and $48 \rightarrow 51$.

The gas phase bands, calculated at 215.34/210.32 nm of the TRANS/CIS conformers are corresponded with the observed band at 213 and 215 nm in CHX and MCH solutions. Similarly the band, calculated at 208.37 and 209.73 nm in the gas phase of the TRANS and CIS conformers, are corresponded with the observed band at 205 nm (in ethanol solution). By examining the orbital transitions and calculated oscillator strengths, these bands are assigned as $\pi \rightarrow \pi^*$ bands.

Any way the observed band centers around 350, 280, 266, 250, 240, 230, 215 and 205 nm are respectively corresponded with the transitions appearing from the ground state $|G\rangle$ to different excited states $|S_1\rangle$, $|S_2\rangle$, $|S_3\rangle$, $|S_4\rangle$, $|S_5\rangle$, $|S_6\rangle$, $|S_7\rangle$ and $|S_8\rangle$ i.e. $G \rightarrow S_1$, $G \rightarrow S_2$, $G \rightarrow S_3$, $G \rightarrow S_4$, $G \rightarrow S_5$, $G \rightarrow S_6$ and $G \rightarrow S_7$ and $G \rightarrow S_8$.

3.4. Raman Excitation Profile Study

When the excitation is much away from resonance, the intensity of a Raman band of frequency (v_a), expressed in terms of a quantity proportional to the number of scattered photons, is determined from the following expression [17],

$$I_a = K(v_0 - v_a)^3 \sum_{\rho,\sigma} |\alpha_{\rho,\sigma}|^2 = K(v_0 - v_a)^3 \left[\sum_I F_A \Delta_a^I \frac{v_{IG}^2 + v_0^2}{(v_{IG}^2 - v_0^2)^2} + \sum_{I(J} F_B \frac{v_{IG} v_{JG} + v_0^2}{(v_{IG}^2 - v_0^2)(v_{IG}^2 - v_0^2)} \right]^2 \quad (2)$$

where K is a constant, v_0 is the exciting frequency, v_a is the frequency of the a th mode and $\alpha_{\rho,\sigma}$ is the $\rho\sigma$ th component of the scattering (polarizability) tensor (ρ,σ = x,y,z). Here $v_{IG} = h^{-1}[E_{I0} - E_{G0}]$, *where* $|I\rangle$ *and* $|G\rangle$ are respectively an excited and ground electronic sates, E_{I0} and E_{G0} are the energies of the lowest vibrational states of the respective electronic states and $|J\rangle$ is another excited electronic state. Δ_a^I is the displacement of the potential minimum of the *I*-th electronic state with respect to the ground state along the concerned (Q_a-th) normal coordinate. F_A and F_B are given by,

$$F_A = \tfrac{2}{ch}(M_\rho)_{GI}^0 (M_\sigma)_{IG}^0, \quad (a)$$
$$F_B = \tfrac{2}{(ch)^2} \left\{ (M_\rho)_{GI}^0 h_{IJ}^a (M_\sigma)_{JG}^0 + (M_\rho)_{GJ}^0 h_{JI}^a (M_\sigma)_{IG}^0 \right\} \langle 1|Q_a|0\rangle \quad (b)$$
$$h_{IJ}^a = \langle I|\partial H/\partial Q_a|J\rangle_0 \quad (c) \quad (3)$$

where the symbols have their usual meaning. The first term in the square bracket in Eq. (2) corresponds to the A-term (FC) and the second term corresponds to the B-term (HT/vibronic coupling). The contribution of the A-term depends on the molecular distortion Δ_a^I and that of the B-term depends on the matrix h_{IJ}^a which mixes the two excited states $|I\rangle$ and $|J\rangle$ through the *a*-th normal mode gradient of the electronic Hamiltonian (H) at the equilibrium configuration. Thus non-zero A-term contribution implies a displacement of the excited state potential minimum along the concerned normal coordinate with respect to the ground state. Symmetry considerations require that such a displacement in the Franck–Condon enhancement mechanism can occur only for totally symmetric vibrational modes,

Table 5 Experimental and theoretical[TD-DFT//B3LYP/6-311G(d, p)] vertical one-electron excitations of 3-BOP (CIS) in different environments

GAS				Cyclohexane (Expt.)				Ethanol (Expt.)				Assignment	
nm	*f*-value	Transition	C.I. co-eff.	nm	*f*-value	Transition	C.I. co-eff.	nm	*f*-value	Transition	C.I. co-eff.		
350.95	0.0002	44 → 49	0.21,875	347.50	0.0002	44 → 49	0.22419	337.28	0.0002	44 → 49	0.23939	$(n\rightarrow\pi^*)$	S_1
		48 → 49	0.61902	(348)		48 → 49	0.61718	(339)		48 → 49	0.58359		
294.78	0.0003	44 → 49	−0.27903	292.39	0.0003	44 → 49	−0.29861	286.94	0.0007	44 → 49	0.29476	$(n\rightarrow\pi^*)$	S_2
		45 → 49	−0.23016	(282)		45 → 49	−0.28503	(274)		45 → 49	0.29244		
		47 → 49	0.53745			47 → 49	0.50746			47 → 49	0.51427		
271.15	0.0019	46 → 49	0.59527	274.02	0.0018	46 → 49	0.56236	279.42	0.0016	44 → 49	0.24677	$(\pi\rightarrow\pi^*)$	S_3
				(266)		47 → 49	−0.25972	(266)		45 → 49	0.26014	^1L_b	
										46 → 49	0.39810		
										47 → 49	−0.36757		
261.43	0.0405	45 → 49	0.57390	263.34	0.0393	45 → 49	0.51754	267.72	0.0403	45 → 49	−0.40313	$(\pi\rightarrow\pi^*)$	S_4
		46 → 49	0.20353	(250)		46 → 49	0.27670	(254)		46 → 49	0.45969	^1L_a	
						47 → 49	0.24578						
250.65	0.0040	44 → 49	0.48288	250.93	0.0049	44 → 49	0.48055	252.08	0.0052	44 → 49	0.45267	$(\pi\rightarrow\pi^*)$	S_5
		47 → 49	0.25699	(241)		47 → 49	0.21320	(239)		45 → 49	−0.32394	^1L_a	
230.34	0.0084	43 → 49	0.36372	229.54	0.0083	43 → 49	−0.31135	230.86	0.0086	43 → 49	0.26895	$(\pi\rightarrow\pi^*)$	S_6
		44 → 50	0.26389	(229)		44 → 50	−0.21423	(230)		44 → 50	0.21054		
		47 → 50	−0.30852			47 → 50	0.36847			47 → 50	0.28793		
		48 → 51	−0.26201			48 → 51	0.31627			48 → 50	0.35030		
										48 → 51	0.26340		
210.32	0.0035	45 → 50	0.20958	210.96	0.0066	45 → 51	−0.21743	210.75	0.0115	46 → 51	0.34361	$(\pi\rightarrow\pi^*)$	S_7
		46 → 50	−0.21890	(213)		46 → 51	0.42358			47 → 51	0.20947		
		46 → 51	0.42570			47 → 50	0.20421			48 → 52	0.37086		
		47 → 52	0.26286			47 → 52	−0.25773						
209.73	0.0224	43 → 49	−0.32923	209.31	0.0201	43 → 49	0.33061	209.35	0.0140	43 → 49	−0.21392	$(\pi\rightarrow\pi^*)$	S_8
		43 → 51	0.27391			43 → 51	−0.27706	(205)		43 → 51	0.20604		
		44 → 50	0.34776			44 → 50	−0.33113			44 → 50	0.38709		
		45 → 50	−0.29709			45 → 50	0.32288			45 → 50	−0.23611		
										48 → 52	0.22913		

Table 5 continued

GAS				Cyclohexane (Expt.)				Ethanol (Expt.)				Assignment	
nm	*f*-value	Transition	C.I. co-eff.	nm	*f*-value	Transition	C.I. co-eff.	nm	*f*-value	Transition	C.I. co-eff.		
158.23	0.0505	45 → 53	−0.27393	158.59	0.0478	45 → 53	−0.23667	159.11	0.0420	45 → 53	0.24889	($\pi \rightarrow \pi^*$)	S_9
		46 → 53	0.48397			46 → 53	0.49630			46 → 53	0.34432		
										46 → 54	0.28133		
										47 → 53	−0.27155		
156.64	0.0381	45 → 53	0.44372	156.70	0.0371	45 → 53	0.44944	157.49	0.0472	45 → 53	0.35476		
		45 → 54	0.21722			46 → 53	0.30323			46 → 53	−0.24084		
		46 → 53	0.28786							46 → 54	−0.25572		
										47 → 54	−0.23762		
										48 → 54	0.21899		

and no non-totally symmetric mode can be expected to undergo Franck–Condon scattering process.

B-term involves vibronic (VC or HT) coupling of the excited state $|I\rangle$ with another excited state $|J\rangle$. For the matrix element $\langle I|\partial H/\partial Q_a|J\rangle_0$ to be non vanishing, the irreducible representation of the vibrational fundamental with normal coordinate Q_a (also of $\partial H/\partial Q_a$) must be contained in the direct product of the irreducible representations of the states $|I\rangle$ and $|J\rangle$. Thus, the B-term can be non-zero for both totally symmetric and non-totally symmetric fundamentals. Even if the states, $|I\rangle$ and $|J\rangle$ are nearer to each other, the above rule has to be followed in order to have non vanishing value of the coupling element $\langle I|\partial H/\partial Q_a|J\rangle_0$. In such case the molecule will be distorted along Q_a. On the other hand, the electric dipole moment selection rule affirms that for totally symmetric vibration, these two favorable excited states always belong to the same symmetry species and the PESs repel. This repulsion gives rise to change in the shape of the respective PESs and therefore in the vibrational frequencies [18]. The strength of the coupling depends on the energy gap between the coupled states. In extreme cases, for very strong coupling, the curvature of the PES of the lower curve may be inverted and double minima may arise. In such case, both totally and non-totally symmetric vibrations may be responsible for vibronic coupling provided the symmetry property of the product, mentioned above, is satisfied.

Generally, the effect of the B-term is smaller than that of the A-term. The relative contribution of B-term is found to increase as the excitation wavelength is more and more away from an allowed electronic transition. In the present case as the exciting radiations are away from resonance, the contributions of both the terms may be important. In some cases interference between the A- and B- terms become important as discussed by Mitra et al. [19] and Albrecht et al. [20].

Both the calculated and observed REPs of several normal modes of vibration of 3-BOP molecule are exhibited in Fig. 6. The observed profiles in chloroform and carbon-tetrachloride solutions at room temperature (around 30 °C) are presented by symbols. The theoretically determined REPs i.e. the diagonal (A-term) and the off-diagonal (B-term) contributions from different excited electronic states (EESs) and also the $(\nu_o - \nu_a)^3$ dependence for classical contributions are represented by solid curves accordingly marked to indicate the contributors. Another point, worth mentioning here, is that as $n \rightarrow \pi^*$ transitions (around 350 and 290 nm) are very weak, no significant contribution is expected from these states (S_1 and S_2) and hence they are not shown in the Fig. 6. This is also the case for the states S_3 and S_7. Moreover, the diagonal contribution from the state S_5 and off-diagonal contribution from the pair of states S_4 & S_6 lie so close to each other that it becomes

Table 6 Experimental and theoretical[TD-DFT//B3LYP/6-311G(d, p)] vertical one-electron excitations of 3-BOP (TRANS) in different environments

GAS				CYCLOHEXANE (Expt.)				ETHANOL (Expt.)				ASSIGNMENT	
nm	*f*-value	Transition	C.I. co-eff.	nm	*f*-value	Transition	C.I. co-eff.	nm	*f*-value	Transition	C.I. co-eff.		
350.39	0.0001	48 → 49	0.62458	347.24 (348)	0.0001	48 → 49	0.61699	337.05 (339)	0.0001	48 → 49	0.55882	($n \rightarrow \pi^*$)	S_1
290.06	0.0004	44 → 49	−0.36652	288.44	0.0004	44 → 49	−0.39645	284.25	0.0009	44 → 49	0.46528	($n \rightarrow \pi^*$)	S_2
		47 → 49	0.46134	(282)		47 → 49	0.43862	(274)		47 → 49	0.24370		
274.58	0.0030	46 → 49	0.64564	276.98	0.0028	46 → 49	0.64155	282.32	0.0025	46 → 49	0.42710	($\pi \rightarrow \pi^*$)	S_3
				(266)				(266)		47 → 49	0.44496	^1L_b	
										48 → 49	0.25842		
262.68	0.0360	45 → 49	0.52786	264.40	0.0361	45 → 49	0.48679	268.26	0.0382	45 → 49	0.41198	($\pi \rightarrow \pi^*$)	S_4
		47 → 49	−0.34685	(250)		47 → 49	−0.38702	(254)		46 → 49	−0.25427	^1L_a	
										47 → 49	0.35199		
252.69	0.0080	44 → 49	0.47747	252.94	0.0080	44 → 49	0.43735	256.02	0.0085	44 → 49	0.36902	($\pi \rightarrow \pi^*$)	S_5
		45 → 49	0.20782	(241)		45 → 49	0.26029	(239)		45 → 49	0.41153	^1L_a	
		47 → 49	0.22568										
234.54	0.0088	43 → 49	0.51941	234.27	0.0118	43 → 49	0.49456	234.41	0.0091	43 → 49	0.57476	($\pi \rightarrow \pi^*$)	S_6
		45 → 50	−0.23719	(229)		45 → 50	−0.21727	(230)		45 → 50	−0.26352		
215.34	0.0047	46 → 50	0.62477	216.90	0.0006	46 → 50	0.48925	217.55	0.0047	46 → 50	0.32015	($\pi \rightarrow \pi^*$)	S_7
				(213)		47 → 51	−0.28412			47 → 51	−0.27420		
208.37	0.0157	43 → 49	0.25827	208.16	0.0167	43 → 49	0.25445	207.72	0.0145	43 → 49	0.20179	($\pi \rightarrow \pi^*$)	S_8
		43 → 51	−0.28338			43 → 51	−0.27988	(205)		43 → 51	−0.21555		
		44 → 50	0.37258			44 → 50	0.37151			44 → 50	0.35462		
		44 → 51	0.26470			44 → 51	0.25024			44 → 51	0.25476		
		45 → 50	0.24680			45 → 50	0.26427			45 → 50	0.25936		
158.28	0.0529	46 → 53	0.53534	158.51	0.0592	46 → 53	0.55011	159.01	0.0567	46 → 53	0.30725	($\pi \rightarrow \pi^*$)	S_9
										47 → 53	0.37387		
										47 → 54	−0.20136		
156.42	0.0146	38 → 49	0.33945	156.43	0.0163	38 → 49	−0.24782	155.55	0.0117	38 → 49	−0.29942		
		42 → 52	−0.21076			39 → 50	0.20565			44 → 53	0.24428		
		44 → 53	−0.34424			41 → 50	−0.23872			45 → 53	0.40464		
						42 → 52	0.26006						
						44 → 53	0.28170						

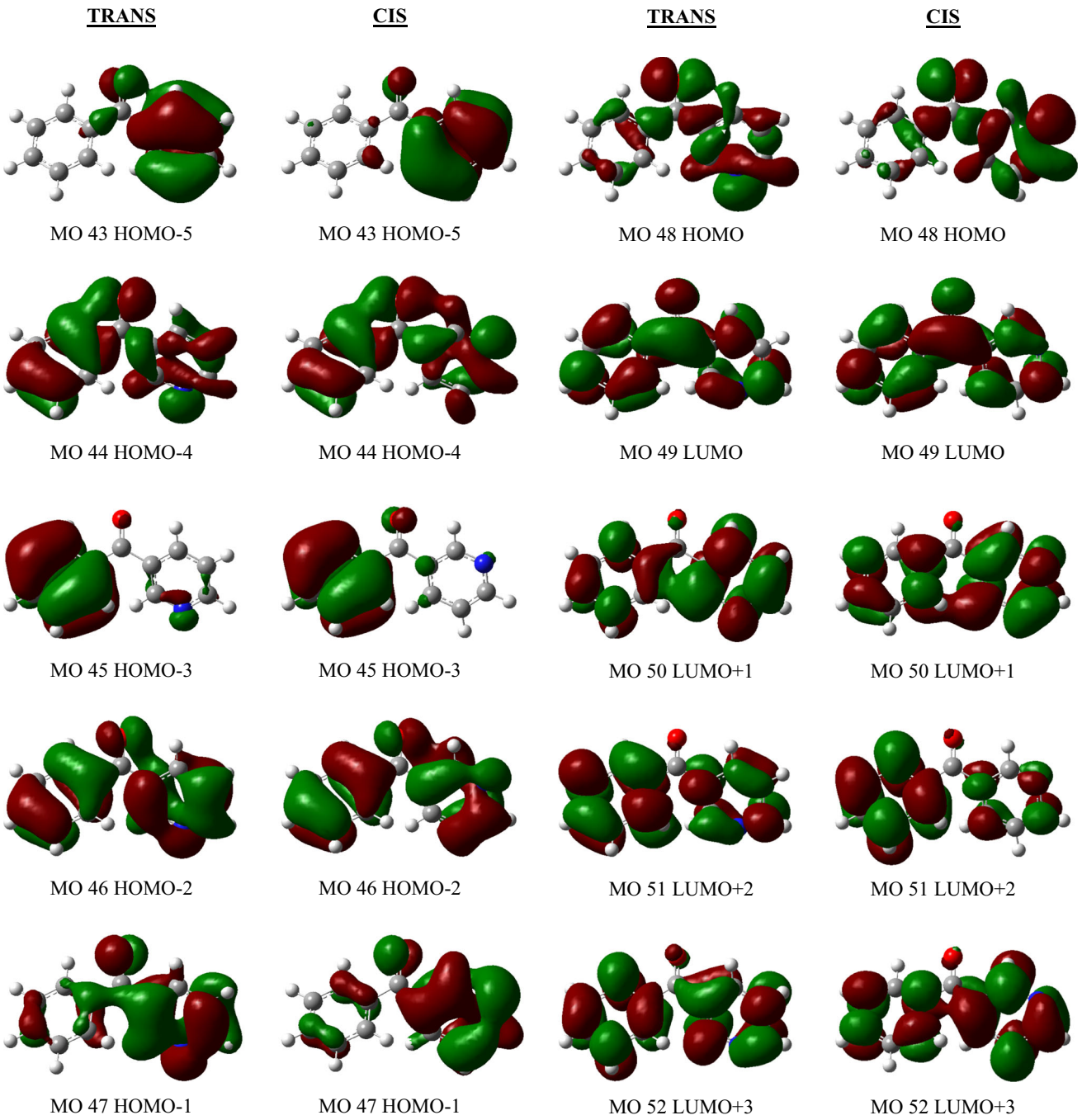

Fig. 5 Electron density contours for selected molecular orbitals of TRANS and CIS conformers of 3-BOP

very difficult to resolve their individual contributions in the REP studies (Fig. 6). The effect of the line width on REPs has been checked as before [6, 7], but no significant effect has been observed. Theoretical A- and B- term scattering intensities of different bands are normalized relative to those for the exciting wavelength at 514.5 nm according to Eq. (2). These theoretical relative intensities are compared with the experimental ones determined from Eq. (1). The accuracy in the measurements of intensities of different Raman bands varies, but REP values are confined within the error ± 5%.

The wavenumber of the C=O stretching mode of the said molecule lies around 1663 cm^{-1}. Critical examination of REP of this mode indicates that the favourable contribution comes from the state S_5 and S_6 through the A-term. The dominating A-term contributions indicate that the molecule is distorted accordingly along this mode in these states i.e. the C=O bond length is changing significantly in these

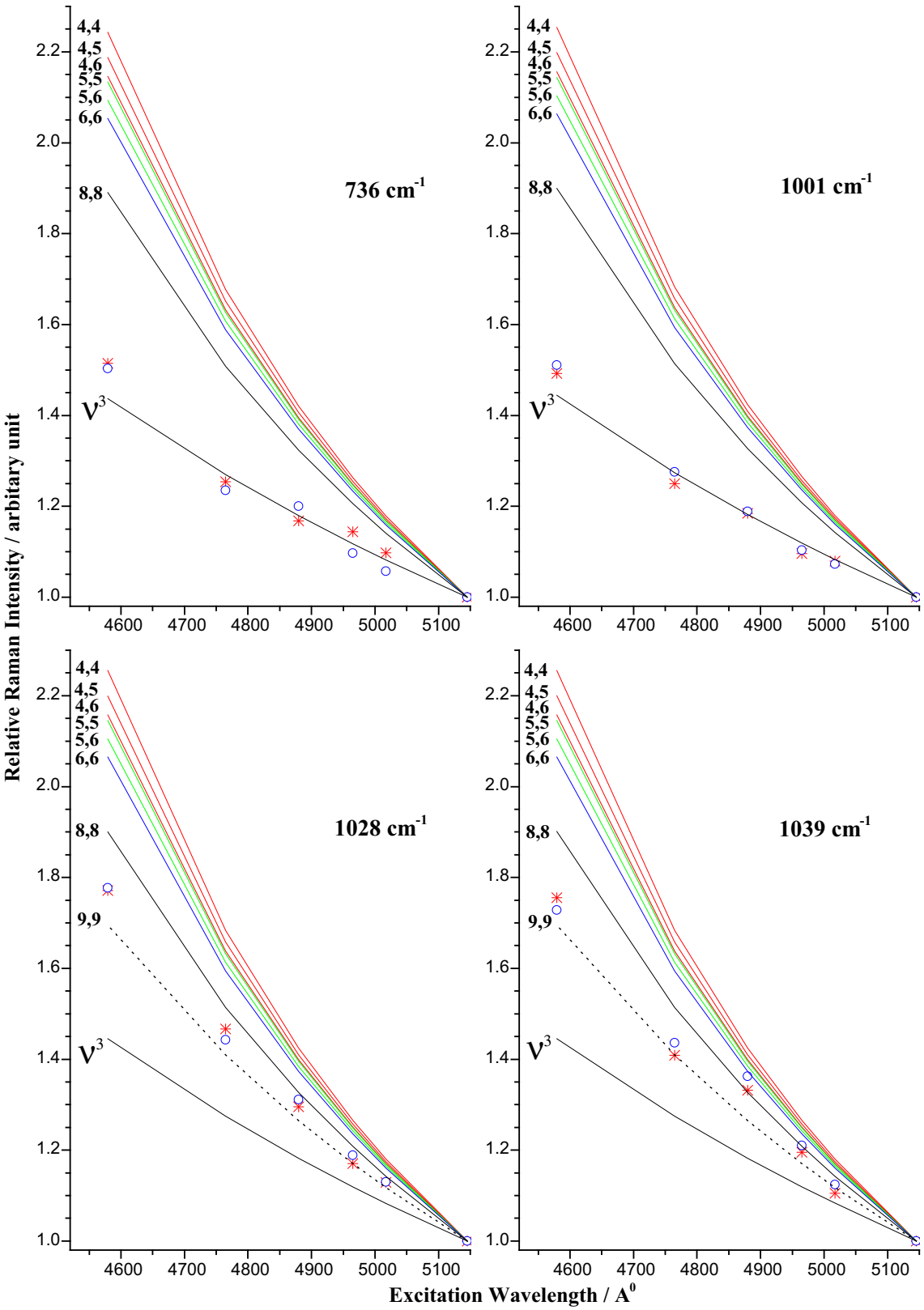

Fig. 6 Measured and calculated REPs for 3-BOP. The symbols ('*' and 'o') indicate the measured profiles in $CHCl_3$ and CCl_4 solutions, respectively. ν^3 denotes classical calculated profiles considering $(\nu_a - \nu_o)^3$ dependence only. (I, J) denotes calculated profile considering contribution from S_I & S_J electronic states. (I = J) denotes A-term contribution and (I ≠ J) denotes B-term contribution and interference between two A-terms

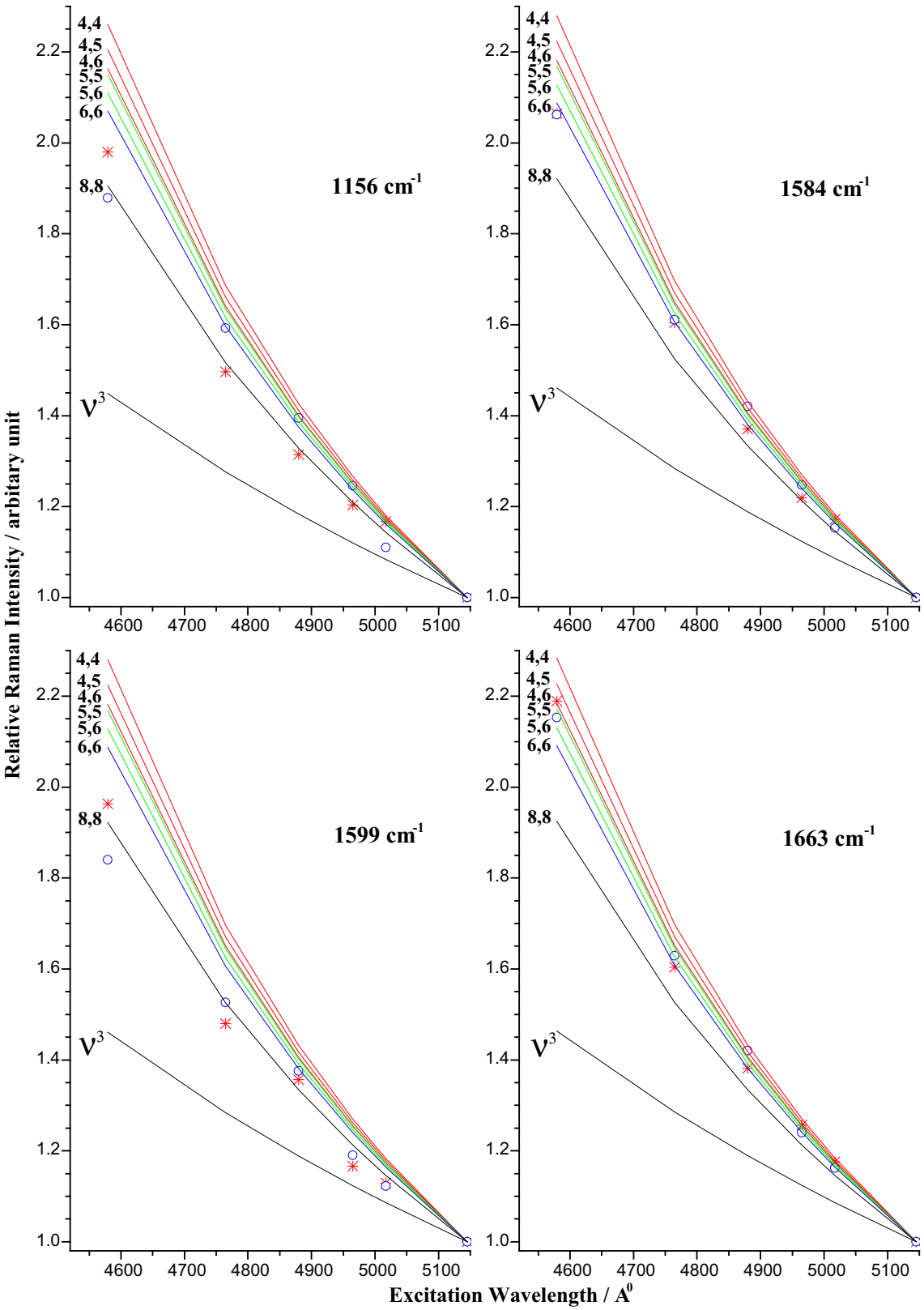

Fig. 6 continued

states. This is in compliance with molecular orbital calculation, where a good contribution to the G → S_5 band comes from the orbital transition 44 → 49, where a major n → π* is involved. Apart from these contributions, this mode also gets possible B-term contributions, which mix the states (S_4 & S_6) and (S_5 & S_6). Existence of strong vibronic coupling among these states suggests that the symmetries of the relevant states remain the same.

Two pyridyl ring triangular modes appear at 736 and 1001 cm^{-1}. REPs of both the bands are more or less similar in nature, though none of the experimentally observed excited electronic states (S_4, S_5, S_6 or S_8) contributes to this mode through A- or B-term of the scattering tensor in each of the two solvents ($CHCl_3$ and CCl_4). But the classical contribution agrees very well with the experimental observation. It means that these vibrations might be getting intensity contributions from the electronic states lying very high in the energy scale.

There are other two strong and polarized Raman bands around 1030 cm^{-1} (at 1028 and 1039 cm^{-1}). Out of these, the former is the CH-bending mode (having significant contributions from the ring stretching vibration, specially $C_{10}C_{11}$ and $C_{11}C_{12}$ stretching) of the phenyl ring and the last one is pyridyl ring breathing mode ($\nu_{CC/CN}$). REPs of both bands indicate that not only the excited electronic states (S_1 to S_8) but also the classical dependence do not agree very well with the experimental observation. The observed profiles of these modes lie between the profiles of the classical contribution and of the electronic state S_8 through A-term. A higher electronic state lying well above S_8 might be the better contributor. Such a state (S_9) around 160 nm gives a good fit (Fig. 6) to the profiles of these modes. In fact theoretically we have found two closely lying strong bands arising mainly from the vertical transitions 45 → 53 and 46 → 53 lying in this region around 158 nm (Tables 5, 6). The A-term scattering from this state and B-term scattering from the pair of states S_8 and S_9 might be ideal for the intensification of these bands.

It has been possible to measure the REP of another phenyl CH-bending mode near 1156 cm^{-1}. REP of this vibration indicates that the excited states S_6 and S_8 are the chief contributors through A-term, however the profile shows some solvent effect. In carbon tetrachloride solution the former state and in chloroform environment the latter one are found to be the better contributors. This indicates that along this mode the potential minima of the molecule undergo appreciable displacements due to excitation from the ground to the S_6 or S_8 state in the respective solvents. Molecular distortion along this mode can be expressed as the shift parameter Δ_a^I, where $\Delta_a^I = L^{-1}\Delta\Re$, L being the transformation matrix from normal to internal coordinate system.

The REPs of CC/CN stretching modes have been measured for some of the comparatively intense bands. Two such strong and polarized Raman bands are observed near 1584 and 1599 cm^{-1} of pyridyl and phenyl ring respectively. The chief contributors to these modes are respectively the states, S_6 and S_8 through A-term.

The chief orbital transitions associated with the S_5-band (experimentally observed around 240 nm), are 44 → 49 and 47 → 49. The first transition is associated with the π-electronic charge redistribution over the two ring moieties. In the other transition, the charge cloud, concentrating mainly over the phenyl ring, becomes less dense and is spread over both the rings after the transition. These have an overall effect of strengthening and weakening of the CC/CN bonds of the pyridyl and phenyl rings respectively. Moreover, the reduction of charge density over the carbonyl group, arising from the transition 44 → 49, particularly, loosens the CO bond and this makes the state S_5 a good contributor to the Raman intensity of this mode which is in agreement with its observed REPs.

Although the orbital transition associated with the S_6-band (observed around 230 nm) is predominantly 43 → 49, another transition 45 → 50 is also noticeable with this band. Similarly the main transition associated with the S_8-band is 44 → 50. In the all these transitions, the charge cloud is so redistributed over the two rings, such that the cloud densities not only over the CC bonds but also over the CH bonds of the phenyl ring change appreciably. As a result A-term contributions from these states to the CH bending vibration (1156 cm^{-1}) of the phenyl ring become important. This observation supports the behaviour of REP of this mode. Again the transition 43 → 49 also weakens the charge cloud over the pyridyl ring which extends its ring bonds. As a result the S_6-state becomes a good contributor to the CC/CN stretching mode (1584 cm^{-1}) of this ring in compliance with the observed profile of this mode.

The dominant orbital transition associated with the S_8 band (around 205 nm) is 44 → 50. This transition increases the bond lengths $C_9C_{10}/C_{12}C_{13}$ of the phenyl ring and decreases the bond lengths $C(N)_2C_3/C_3N(C)_4$ of the pyridyl ring. This observation agrees well with the observed profiles of the stretching modes of the phenyl (1599 cm^{-1}) and pyridyl (1039 cm^{-1}) rings and also with the respective PEDs.

4. Conclusions

In the present paper detailed spectroscopic investigations on 3-BOP molecule have been carried out and structural changes encountered by the molecule on excitation to different low lying electronic excited states have been

investigated which is supposed to help in studying the photophysics and photochemistry of the molecule. All the experimental findings are aided by quantum chemical calculations. The molecule is found to exist in two stable conformers, CIS and TRANS of which the latter is found to be more stable where the angle between the two ring planes is found to be 51°. Complete vibrational assignment and detailed electronic spectral studies have been carried out to explain the measured Raman excitation profiles of several normal modes. The electronic band at 240 nm is found to have an overall effect of strengthening and weakening of the CC/CN bonds of the pyridyl and phenyl rings respectively and also of loosening the CO bond. Besides this an interesting thing is found from Raman excitation profile studies. An electronic band lying around 160 nm is found to play an important role on the Raman scattering phenomenon which is complemented by theoretical calculation.

Acknowledgements Pinaky Sett expresses thanks to UGC, Government of India, for financial support through the minor research project (MRP Project No.—F. PSW-156/13-14).

References

[1] E Castellucci, L Angeloni, G Marconi, E Venuti and I Baraldi *J. Phys. Chem.* **94** 1740 (1990)
[2] E C Lim *Radiation less Transition in Excited States* (NewYork: Academic Press) (eds) E C Lim Vol 3 (1974)
[3] T Mishra *et al*. *Spectrochim. Acta A Mol. Biomol. Spectrosc.* **74** 1165 (2009)
[4] S C Shim, D W Kim and M S Kim *J. Photochem. Photobiol A: Chemistry* 56 227 (1991)
[5] C Dubroca and P Lozano *Chem. Phys. Lett.* **24** 49 (1974)
[6] P Sett, T Misra, S Chattopadhyay, A K De and P K Mallick *Vibrational Spectrosc.* **44** 331 (2007)
[7] P Sett *et al*. *J. Chem. Phys.* **128** 144507 (2008)
[8] S Datta, P Sett, J Chowdhury, M Ghosh and P K Mallick *Applied Spectrosc.* **67** 1447 (2013)
[9] P Sett, S Datta and P K Mallick *J. Raman Spectrosc.* **42** 859 (2011)
[10] M J Frisch *et al*. *Gaussian 03, Revision B.03.* (Pittsburg : Gaussian Inc.), (2003)
[11] J M L Martin and C V Alsenoy *GAR2PED* (Belgium : University of Antwerp) (1995)
[12] V Volvosek, G Baranovic, L Colombo and J R Durig *J. Raman Spectrosc.* **22** 35 (1991)
[13] I Baraldi, E Gallinella and M Scoponi *Spectrochim. Acta A Mol. Biomol. Spectrosc.* **43** 1045 (1987)
[14] J E Katon, W R Feairheller and E R Lippincott *J. Mol.Spectrosc.* **13** 72 (1964)
[15] F A Mautner and M A Goher *Polyhedron.* **18** 553 (1998)
[16] J Chaudhuryn and M Ghosh *J. Raman Spectrosc.* **35** 1023 (2004)
[17] A C Albecht *J. Chem. Phys.* **34** 1476 (1961)
[18] J F Arenas, M S Woolley, I L Tokon, J C Otero and J I Marcos *J. Chem. Phys.* **112** 7669 (2000)
[19] A Mitra and P K Mallick *Indian J. Phys.* **68B** 47 (1994)
[20] A C Albrecht and M C Hutley *J. Chem. Phys.* **55** 4438 (1971)